Journal of Medicinal Chemistry

The Identification of Potent, Selective and Orally Available Inhibitors of Ataxia Telangiectasia Mutated (ATM) Kinase: The Discovery of AZD0156 (8-{6-[3-(dimethylamino)propoxy]pyridin-3-yl}-3-methyl-1-(tetrahydro-2H-pyran-4-yl)-1,3-dihydro-2H-imidazo[4,5-c]quinolin-2-one)

Kurt G. Pike, Bernard Barlaam, Elaine Cadogan, Andrew Campbell, Yingxue Chen, Nicola Colclough, Nichola L Davies, Camila DeAlmeida, Sébastien L. Degorce, Myriam Didelot, Allan Dishington, Richard Ducray, Stephen T. Durant, Lorraine A. Hassall, Jane L. Holmes, Gareth D Hughes, Philip A MacFaul, Keith R. Mulholland, Thomas M. McGuire, Gilles Ouvry, Martin Pass, Graeme R. Robb, Natalie Stratton, Zhenhua Wang, Joanne Wilson, Baochang Zhai, Kang Zhao, and Nidal Al-Huniti

J. Med. Chem., **Just Accepted Manuscript** • DOI: 10.1021/acs.jmedchem.7b01896 • Publication Date (Web): 23 Apr 2018

The Identification of Potent, Selective and Orally Available Inhibitors of Ataxia Telangiectasia Mutated (ATM) Kinase: The Discovery of AZD0156 (8-{6-[3-(dimethylamino)propoxy]pyridin-3-yl}-3-methyl-1-(tetrahydro-2H-pyran-4-yl)-1,3-dihydro-2H-imidazo[4,5-c]quinolin-2-one)

Kurt G. Pike,[1] Bernard Barlaam,[1] Elaine Cadogan,[1] Andrew Campbell,[2] Yingxue Chen,[3] Nicola Colclough,[1] Nichola L. Davies,[1] Camila de-Almeida,[1] Sebastien L. Degorce,[1,6] Myriam Didelot,[6] Allan Dishington,[4] Richard Ducray,[6] Stephen T. Durant,[1] Lorraine A. Hassall,[4] Jane Holmes,[4] Gareth D. Hughes,[1] Philip A. MacFaul,[4] Keith R. Mulholland,[5] Thomas M. McGuire,[1] Gilles Ouvry,[6] Martin Pass,[1] Graeme Robb,[1] Natalie Stratton,[7] Zhenhua Wang,[8] Joanne Wilson,[1] Baochang Zhai,[8] Kang Zhao,[8] Nidal Al-Huniti.[3]

[1] Oncology, IMED Biotech Unit, AstraZeneca, Building 310, Cambridge Science Park, 319 Milton Road, Cambridge CB4 0WG, UK. [2] Pharmaceutical Sciences, AstraZeneca, Silk Road Business Park, Macclesfield, SK10 2NA, UK. [3] Oncology, IMED Biotech Unit, AstraZeneca, 35 Gatehouse Drive, Waltham, MA 02451, USA. [4] Oncology, IMED Biotech Unit, AstraZeneca, Alderley Park, Macclesfield, Cheshire SK10 4TG, UK [5] Chemical Development, AstraZeneca, Silk Road Business Park, Macclesfield, SK10 2NA, UK. [6] Oncology, IMED Biotech Unit, AstraZeneca, Centre de

Recherches, Z.I. la Pompelle, BP 1050, 51689 Reims Cedex 2, France. [7] Discovery Sciences, AstraZeneca, Alderley Park, Macclesfield, Cheshire SK10 4TG, UK. [8] Pharmaron Beijing Co., Ltd., 6 Taihe Road BDA, Beijing, 100176, P.R. China.

ABSTRACT

ATM inhibitors, such as **7**, have demonstrated the anti-tumor potential of ATM inhibition when combined with DNA double strand break-inducing agents in mouse xenograft models. However, the properties of **7** result in a relatively high predicted clinically efficacious dose. In an attempt to minimize attrition during clinical development we sought to identify ATM inhibitors with a low predicted clinical dose (<50 mg) and focussed on strategies to increase both ATM potency and predicted human pharmacokinetic half-life (predominantly through the increase of volume of distribution). These efforts resulted in the discovery of **64** (AZD0156), an exceptionally potent and selective inhibitor of ATM based on an imidazo[4,5-c]quinolin-2-one core. **64** has good preclinical phamacokinetics, a low predicted clincal dose and high maximum absorbable dose. **64** has been shown to potentiate the efficacy of the approved drugs irinotecan and olaparib in disease relevant mouse models and is currently undergoing clinical evaluation with these agents.

INTRODUCTION

The DNA within our cells is constantly under attack from endogenous sources, environmental mutagens and carcinogens with tens of thousands of DNA damage events occurring every day.[1,2] To effectively detect and repair the different types of DNA damage incurred the body has developed a suite of different repair mechanisms and signaling pathways, collectively termed the DNA damage response (DDR).[3] Although not the most frequent form of DNA damage, DNA double-strand breaks (DSBs) are the most cytotoxic and are repaired by either the homologous recombination repair (HRR) pathway or the non-homologous end-joining (NHEJ) pathway. The HRR pathway is a relatively efficient and

accurate repair pathway for DNA DSBs but requires the presence of undamaged sister chromatid DNA, whereas the NHEJ is less accurate but is not dependent on the presence of replicated DNA.[4,5] Cancer cells typically have high levels of replication stress, defects in one or more DDR pathway and a higher level of endogenous DNA damage resulting from a variety of factors associated with increased proliferation and loss of cell cycle checkpoints. The result of these differences mean that cancer cells are more sensitive to exogenous DNA damage than normal cells and supports the hypothesis that targeting DDR pathways may provide an effective avenue for cancer therapies.[6] The formation of DNA DSBs is the primary driver for the cytotoxicity for a number of approved cancer chemotherapies, such as topoisomerase I and II inhibitors (*e.g.* irinotecan), as well as for ionizing radiation (IR). In addition, DNA DSBs can be induced by targeting specific DDR pathways, such as the inhibition of PARP with the approved drug olaparib. Opportunities to interfere with the repair of DNA DSBs may therefore offer the potential to enhance the cytotoxicity of DSB inducing agents.

Ataxia telangiectasia Mutated (ATM) derives its name from a rare human autosomal recessive disorder ataxia-telangiectasia (A-T) that results from mutations in the ATM gene which causes patients to suffer a variety of symptoms including immunodeficiency, extreme radiosensitivity and a predisposition to cancer.[7] ATM kinase is a member of the phosphatidylinositol 3-kinase (PI3K)-related kinase (PIKK) family of atypical serine/threonine protein kinases (also comprising ATR, DNA-PKcs, mTOR, SMG1 and the non-enzymatic TRRAP) and plays a central role in both the early signaling of, and the protection of cells against, DNA DSBs and reactive oxygen species (ROS) that radiotherapy and a wide range of chemotherapies induce.[8-10] ATM is a large protein (350 kDa) comprising 3056 residues and containing a kinase domain with a relatively high degree of similarity to all isoforms of the lipid kinase PI3K.[11] ATM, in its inactive dimeric form, is recruited to the site of a DNA DSB by the DNA-end tethering MRE11-RAD50-NBS1 (MRN) complex and results in the autophosphorylation of ATM on Serine 1981 and subsequent dimer dissociation.[12,13] The activated ATM monomer phosphorylates a broad range of downstream targets, including γH2AX, p53 Mdm2 and Chk2, thereby initiating a

signaling network capable of activating both cell survival and cell death pathways.[14-18] Loss of ATM activity results in the sensitization of virtually all cells to IR whereas upregulation of ATM signaling has been observed to result in both chemoresistance and radioresistance in cancer cells.[19-21] The central role of ATM in coordinating both the HR and NHEJ repair pathways in response to induced DNA DSBs, and its non-canonical responses to cellular stress, highlights this protein as a highly attractive pharmacological target to sensitize tumor cells to both chemotherapy and radiotherapy.[22-24]

A number of selective inhibitors of ATM have been disclosed the first of which, **2** (KU-55933), was developed by KuDOS Pharmaceuticals (now part of AstraZeneca) following the extensive structure-activity relationship (SAR) studies performed on chemical scaffolds related to the pan-PI3K and pan-PIKK inhibitor **1** (LY294002), figure 1.[25,26] Compound **2** is a potent, ATP-competitive inhibitor of ATM enzyme (IC_{50} = 0.013 μM) with high levels of selectivity over the closely related enzymes DNA-PK (IC_{50} = 2.5 μM), ATR (IC_{50} >100 μM), mTOR (IC_{50} = 9.3 μM) and PI3K (IC_{50} = 17 μM) and has been shown to sensitize HeLa cells to the cytotoxic effects of topoisomerase I and II inhibitors and to IR.[27] The utility of **2** has been limited to *in vitro* assessment as a result of poor physicochemical properties, in particular low aqueous solubility and low oral bioavailability. Subsequent optimization of the scaffold resulted in the discovery of second generation ATM inhibitors, such as **3** (KU-59403), with improved potency and properties.[28] Compound **3** is a potent inhibitor of ATM enzyme (IC_{50} = 0.003 μM) with >300 fold selectivity over ATR, DNA-PK, mTOR and PI3K and showed effective chemosensitization in cells at 1 μM. Despite the improved solubility of **3** the compound remains unsuited to oral administration (PO); however, intraperitoneal administration (IP) has allowed the study of **3** in tumor-bearing mice. Tumor growth delay was observed following administration of **3** (25 mg/kg IP BID) for 5 days when combined with either etoposide or irinotecan. More recently the quinazoline **4** has been reported as a modest inhibitor of ATM in cell-based assays (IC_{50} = 1.2 μM) but with good *in vivo* pharmacokinetics in mouse ($t_{1/2}$ = 19 h).[29] Quinazoline **4** showed efficacy when evaluated at 10 μM in a clonogenic assay in which MCF7 cells were treated with compound and irradiated with increasing

doses of IR (0, 2 and 4 Gy) but concerns about its selectivity remain (significant activity was observed against 41 out of 451 kinases when tested at 3 μM in a panel of diverse kinases).

Figure 1: Structures of LY294002 (**1**), KU-55933 (**2**), KU-59403 (**3**) and quinazoline **4**.

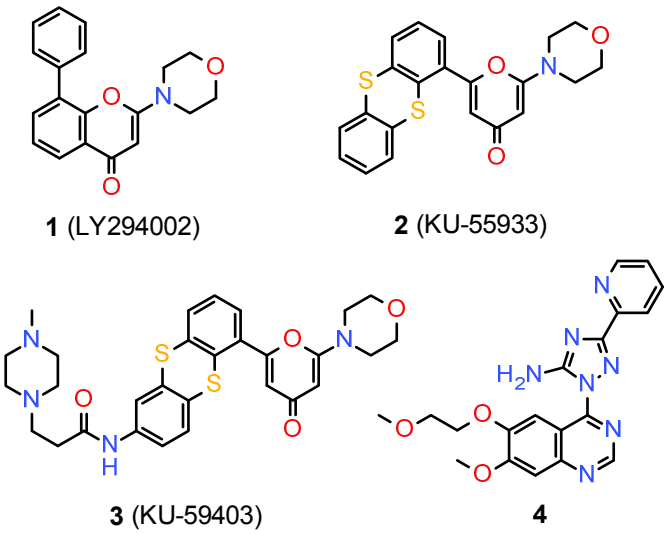

We have recently disclosed the optimization of a quinoline carboxamide scaffold from an initial screening hit **5**, a modestly potent inhibitor in cells with encouraging selectivity over closely related targets, to deliver potent and selective compounds with oral bioavailability, such as **6** (which has been given the external identifier AZ31) and **7**, table 1.[30] Such compounds represent a significant advance allowing the more detailed investigation of ATM inhibition *in vivo*. Compound **6**, administered orally at 100 mg/kg QD, has been shown to potentiate the efficacy of IR in an HT29 mouse xenograft model and the efficacy of irinotecan, administered at 50 mg/kg IP Q7D, in an SW620 mouse xenograft model, resulting in tumor regressions.[31,32] Compound **7**, administered orally at 50 mg/kg BID (on days 2-4 of a weekly schedule), has also been shown to potentiate the efficacy of irinotecan, administered at 50 mg/kg IP Q7D, and cause tumor regression in an SW620 mouse xenograft model.[30] As anticipated, no significant activity in these models was observed for either **6** or **7** in the absence of a DNA DSB-inducing agent. The efficacious doses of **6** and **7** identified provide free plasma concentrations at, or

above, the cellular IC_{50} for ATM for approximately 24 hours in mice on the days that the inhibitors were dosed. This level and duration of target engagement has subsequently been used to define the likely efficacious clinical exposure. The increased separation between ATM potency and potency against the hERG (human ether-a-go-go gene related gene) ion channel suggested a reduced risk of adverse cardiovascular events for compound **7** compared to **6** and its potential as a clinical candidate was assessed.[33]

Table 1: Structure and profiles of screening hit **5** and optimized quinoline carboxamide examples AZ31 (**6**) and **7**.[a]

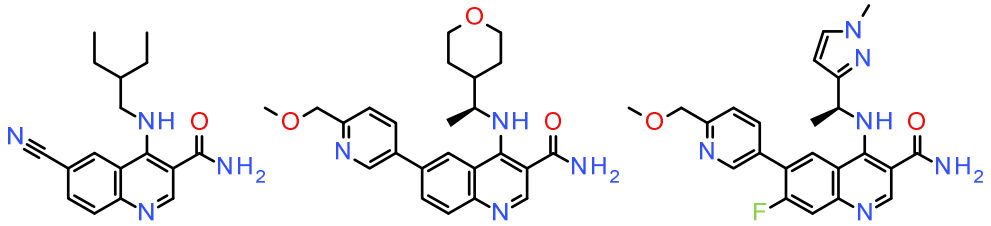

5 **6** (AZ31) **7**

Entry	ATM Cell IC_{50}	ATR Cell IC_{50}	Log$D_{7.4}$	Aq Sol[b]	human / rat heps[c]	hERG IC_{50}
5	0.82	4.4	3.5	19	12 / 74	2.3
6 (AZ31)	0.046	>30	2.5	590	<2.6 / <5.3	4.5
7	0.033	>19	2.7	69	<1.5 / 5.3	22

[a] All IC_{50} data are expressed in micromolar (μM) and ATM / ATR potency values are the geometric mean of at least 3 independent measurements. Further details for the biological assays can be found in the supplemental section.

[b] Thermodynamic aqueous solubility was measured at pH7.4 and the data are expressed in micromolar (μM). No assessment of solid state was made.

[c] The data are expressed in μL/min/10^6 cells

Physiologically-based pharmacokinetic (PBPK) models attempt to portray the body as a series of compartments that represent tissues and organs connected by the arterial and venous blood flow

pathways.[34,35] These models utilize measured physiological data to describe the tissues and organs by their volume and the blood flow to them and can be used to predict the disposition of novel compounds in human. Predicted human pharmacokinetic parameters can be used to simulate the dose required to achieve a target concentration for a defined duration which, when combined with an understanding of the target engagement required for efficacy in preclinical models, can be used to predict the efficacious clinical dose.[36] PBPK modelling suggested that **7** would possess a relatively short half-life in humans (~4 hours) and would, therefore, require an oral dose of 700 mg QD to deliver the desired clinical exposure. The simulation also predicts that a maximum unbound concentration (free C_{max}) of 1.3 μM would be reached following this dose. This relatively high predicted free C_{max} increases the likelihood that non-ATM mediated pharmacology may become manifest thus reducing compound tolerability. Whilst it is appreciated that alternative dosing regimens, for example BID dosing, could be employed in an effort to maintain the desired level and extend of target engagment whilst reducing both total dose and free C_{max}, such regimens are generally considered less attractive as they place increased burden on patients to remain compliant.

Many approaches to minimize compound attrition during clinical development have been suggested and recent analyses have recognized the link between an increased risk of non-target mediated toxicity (including idiosyncratic toxicity) and increasing clinical dose (and by inference increasing free C_{max}).[37,38] As a result of these analyses, where possible, AstraZeneca has adopted the approach of selecting compounds for clinical development which have a low predicted clinically efficacious dose (<50 mg). However, attrition in clinical development is not solely due to toxicity and consideration should also be given to the developability of a clinical candidate. For orally administered compounds the parameter of maximum absorbable dose (D_{abs}) is often used, in conjunction with a predicted clinical dose, to understand whether a significant investment in formulation will be required to achieve the desired exposure. Poor developability can add significant cost and time to the clinical development of a clinical candidate and could limit the achievable clinical exposure preventing the

biological hypothesis from being properly tested.[39-41] Computational simulation software (for example GastroPlus™ or the GI-Sim model) can be used to predict D_{abs} based on easily measured *in vitro* parameters, such as aqueous solubility and permeability, combined with knowledge of intestinal surface area and transit times.[42] In addition to selecting clinical candidates with a low predicted clinically efficacious dose ,where possible, AstraZeneca looks to select candidates with a predicted D_{abs} at least 10-fold above the predicted clinically efficacious dose. As a consequence of good permeability in MDCK cells overexpressing MDR1 (P_{app} A-B = 12 x 10^{-6} cm/s, efflux ratio = 8.7) and moderate aqueous solubility (69 μM), the D_{abs} of **7** was predicted to be approximately 500 mg. Whilst the predicted clinically efficacious dose and D_{abs} would not necessarily preclude the development of **7** as a clinical candidate we sought to continue compound optimization with an emphasis on reducing predicted clinical dose and increasing D_{abs}. Such compounds, we hypothesized, would carry a reduced risk of attrition during clinical development.

CHEMISTRY

Compounds reported herein were synthesized as shown in Schemes 1–6. The versatile 6-bromo-4-chloro-7-fluoroquinoline-3-carboxamide (**10**) was prepared in 4 steps from commercially available 4-bromo-3-fluoroaniline **8**.[30] Reaction of **8** with 1,3-diethyl 2-(ethoxymethylidene)propanedioate, followed by a high temperature cyclisation gave intermediate **9** which could be easily converted to intermediate **10** by hydrolysis, chlorination and amide formation. Suzuki cross-coupling methodology was used to install the required aryl substituent into the 6-position of the quinoline ring to give **11**. S_NAr reaction with the appropriate amine, followed by Hoffman rearrangement[43] and subsequent methylation, gave compounds **12** – **15**. Compounds **18** – **20** were prepared from **10** by employing the same transformations, albeit with the sequence altered. Compound **16** was prepared from **10** by S_NAr reaction with 3-(aminomethyl)pentane followed by Suzuki cross-coupling and a subsequent S_NAr reaction on the resultant fluoropyrimidine, scheme 1.

Scheme 1:[a] Synthesis of **12** – **15**, **16** and **18** - **20**.

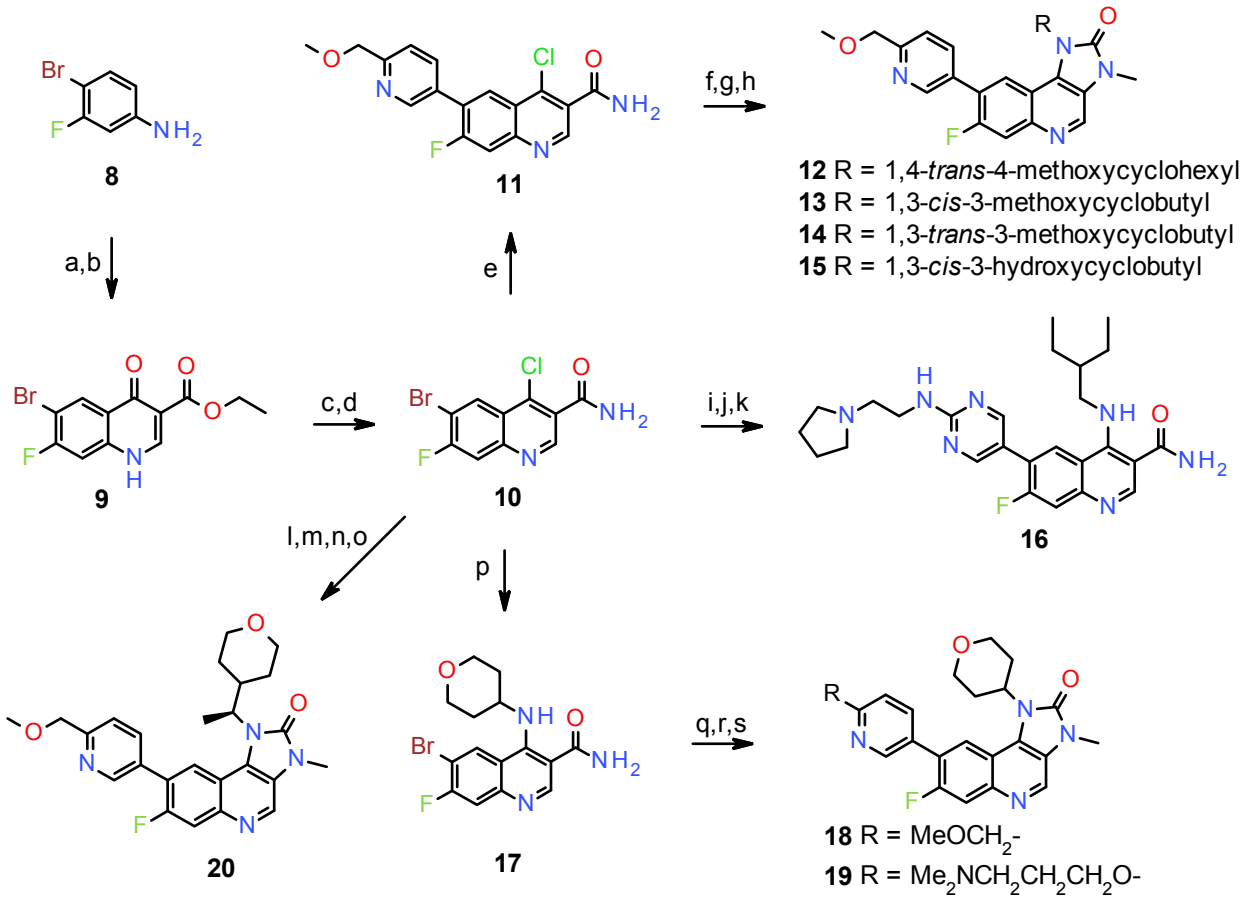

[a] Reagents and conditions: (a) 1,3-diethyl 2-(ethoxymethylidene)propanedioate, EtOH, 80 °C, 4 h (84%); (b) Ph_2O, 240 °C, 2.5 h (64%); (c) NaOH, EtOH, water, 75 °C, 2 h (89%); (d) $SOCl_2$, DMF, 75 °C, 2 h, NH_4OH (100%); (e) aryl boronic acid, Cs_2CO_3, $Pd(PPh_3)_4$, dioxane:water, 90 °C, 4 h (72%); (f) amine, DIPEA, DMA, 30-100 °C, 5-6h (44-72%); (g) trichloroisocyanuric acid, DBU, MeOH, r.t., 0.25-2 h (56-70%); (h) MeI, TBAB, NaOH, DCM, water, r.t., 2.5-24 h, (21-49%); (i) 3-(aminomethyl)pentane, DIPEA, DMA, 100 °C, 5 h (100%); (j) 2-fluoro-5-(tetramethyl-1,3,2-dioxaborolan-2-yl)pyrimidine, Cs_2CO_3, $Pd(PPh_3)_4$, dioxane:water, 95 °C, 3 h (82%); (k) 2-(pyrrolidin-1-yl)ethan-1-amine, DIPEA, DMA, 34 °C, 1 h (80%); (l) (S)-1-(tetrahydro-2H-pyran-4-yl)ethanamine, DIPEA, DMA, 100 °C, 24 h (70%); (m) trichloroisocyanuric acid, DBU, MeOH, r.t., 20 min. (100%); (n) MeI, TBAB, NaOH, DCM, water, r.t., 2.5 h, (98%); (o) aryl boronic acid, Cs_2CO_3, $Pd(PPh_3)_4$, DMF:water, 90 °C, 2 h (37%); (p) tetrahydro-2H-pyran-4-amine, DIPEA, DMA, 100 °C, 24 h (78%); (q) trichloroisocyanuric acid, DBU, MeOH, r.t., 15 min. (98%); (r) MeI, TBAB, NaOH, DCM, water, r.t., 24 h, (26%); (s) aryl boronic acid, Cs_2CO_3, $Pd(PPh_3)_4$, dioxane:water, 80-90 °C, 1.5-2 h (40-74%).

The versatile intermediate ethyl 6-bromo-4-chloro-7-fluoroquinoline-3-carboxylate (**21**) could be easily prepared from **9** by treatment with thionyl chloride. An S_NAr reaction was used to install the methoxycyclobutyl motif, followed by ester hydrolysis, Curtius rearrangement and subsequent methylation to afford **22**. Compounds **24**, **25** and **28** were prepared using Suzuki cross coupling methodology to install a simply substituted pyridyl ring followed by standard manipulations to complete the elaboration of the pyridyl substituent. Miyaura borylation[44] of **22** followed by Suzuki coupling afforded compound **27**. Compounds **29** - **33** were synthesized from intermediate **22** by Suzuki coupling of fully elaborated boronates, scheme 2.

Scheme 2:[a] Synthesis of **24**, **25** and **27** – **33**.

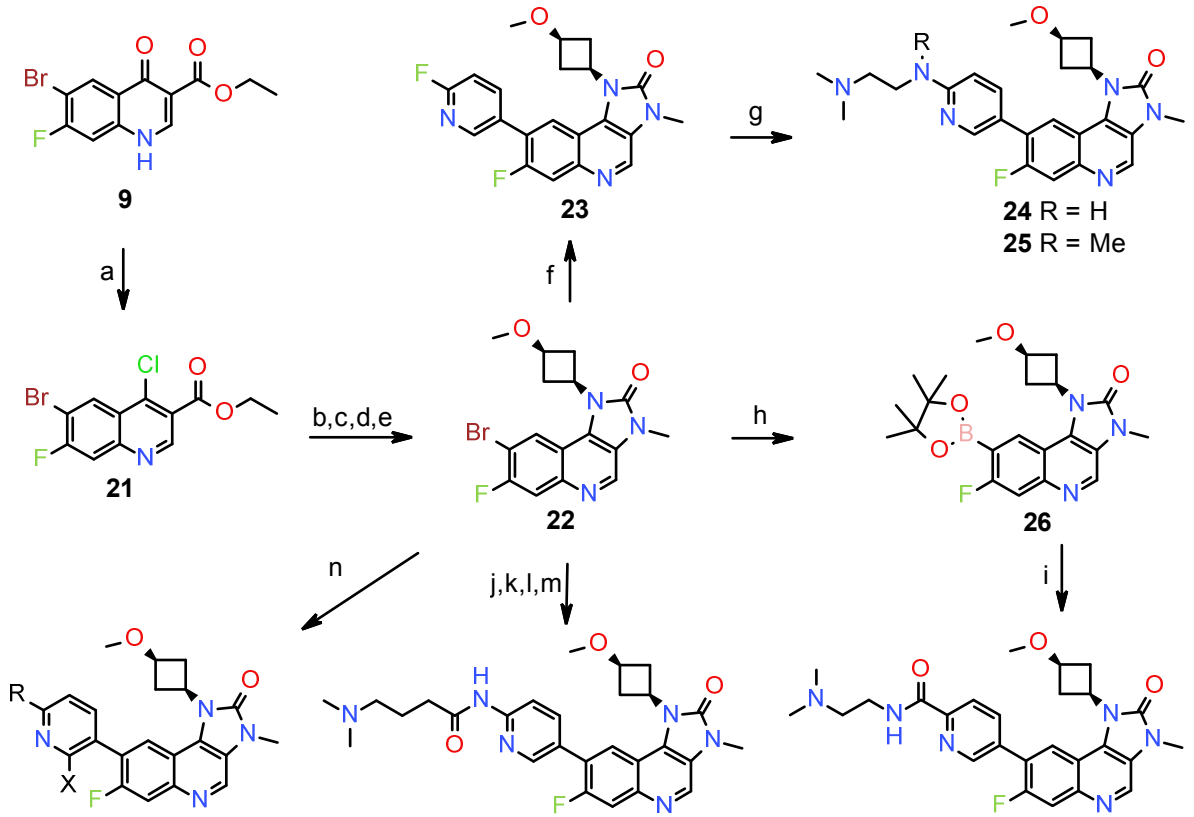

[a] Reagents and conditions: (a) $SOCl_2$, DMF, 80 °C, 4 h (70%); (b) 3-methoxycyclobutan-1-amine.HCl, DIPEA, DMA, 85 °C, 3 h (77%); (c) NaOH, EtOH, water, 40 °C, 2 h (81%); (d) DPPA, TEA, DMF, 60 °C, 2 h, (77%); (e) MeI, TBAB, NaOH, DCM, water, r.t., 24 h, (75%); (f) (6-fluoropyridin-3-yl)boronic acid, Cs_2CO_3, $Pd(PPh_3)_4$, dioxane:water, 90 °C, 3 h; (g) amine, DMSO, 110 °C, 1-2 h (47-54%); (h) B_2Pin_2, (dppf)$PdCl_2$, KOAc, Dioxane , 80 °C, 2 h (76%); (i) aryl boronic acid, Cs_2CO_3, $Pd(PPh_3)_4$, dioxane:water, 80 °C, 2 h (17%); (j) (6-[[(tert-butoxy)carbonyl]amino]pyridin-3-yl)boronic acid, Cs_2CO_3, $Pd(PPh_3)_4$, dioxane:water, 100 °C, 3 h (70%); (k) 4-chlorobutanoyl chloride, DIPEA, DCM, r.t., 16 h (66%). (l) TFA, DCM, r.t., 30 min (99%); (m) dimethylamine, NaI, THF, 60 °C, 16 h, (19%); (n) arylboronic ester, Cs_2CO_3, $Pd(PPh_3)_4$, dioxane:water, 80 °C, 2-6 h (22-62%);.

Analogous transformations employing a Hoffman rearrangement were used to prepare compounds **37** – **40**, **42**, **43**, **45** – **48**, **50** and **51** from 6-bromo-4-chloroquinoline-3-carboxamide (**35**), scheme 3, or using a Curtius rearrangement to prepare compounds **57** – **61**, **63** and **64** from ethyl 6-bromo-4-chloroquinoline-3-carboxylate (**52**), scheme 4. *N*-Oxide **65** was made by the biocatalytic oxidation of **64**, scheme 4.

Scheme 3:[a] Synthesis of 1H-imidazo[4,5-c]quinolin-2(3H)-ones by Hoffmann rearrangement.

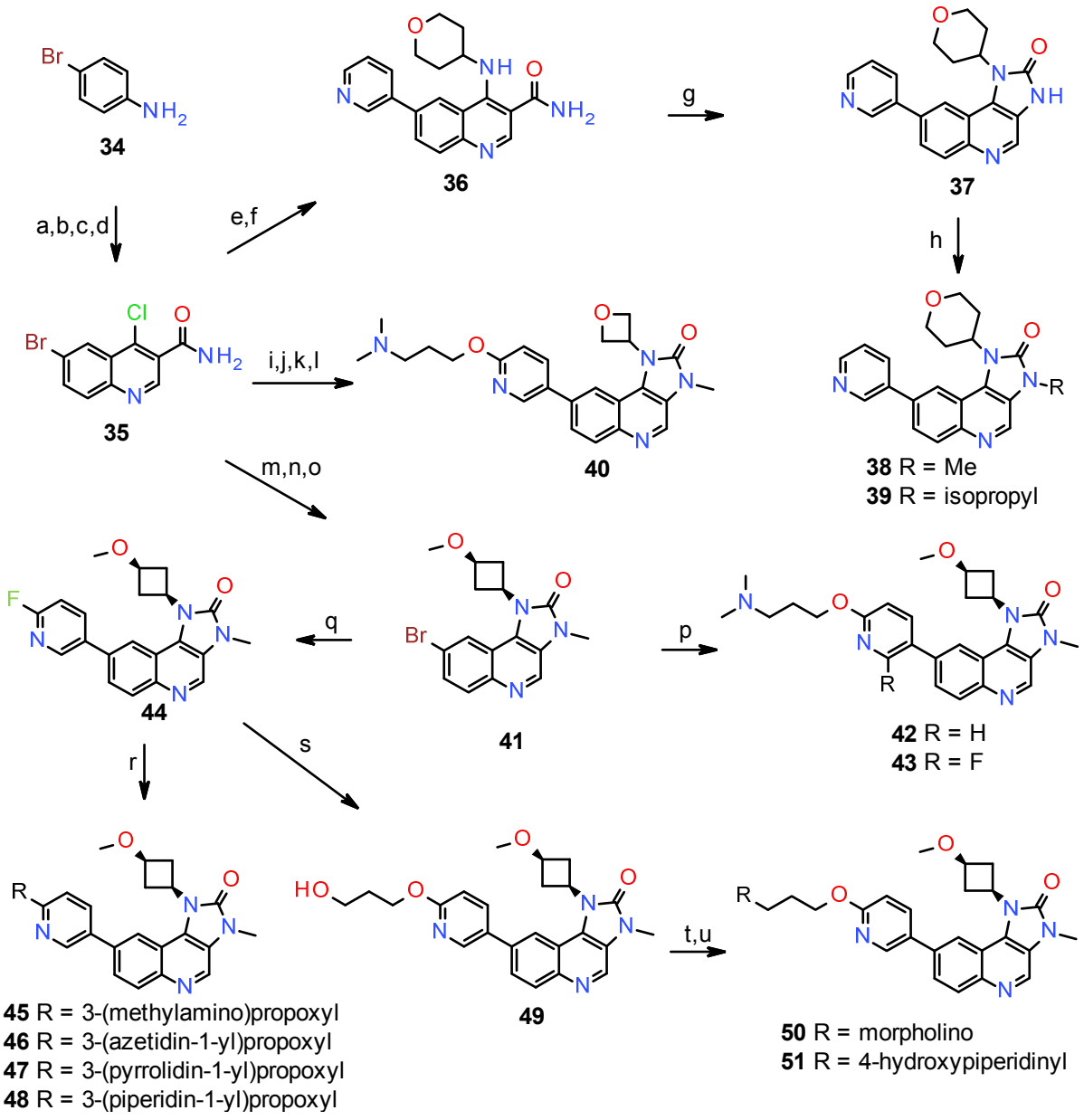

[a] Reagents and conditions: (a) 1,3-diethyl 2-(ethoxymethylidene)propanedioate, EtOH, 78 °C, 24 h (90%); (b) Ph_2O, 240 °C, 1 h; (c) NaOH, EtOH, water, 75 °C, 1.5 h (96%); (d) $SOCl_2$, DMF, 70 °C, 2 h; NH_4OH (95%); (e) 3-(4,4,5,5-tetramethyl-1,3,2-dioxaborolan-2-yl)pyridine, Cs_2CO_3, $Pd(PPh_3)_4$, dioxane:water, 100 °C, 5 h (72%); (f) tetrahydro-2H-pyran-4-amine.HCl, DIPEA, DMF, 80 °C, 16 h (19%); (g) trichloroisocyanuric acid, DBU, MeOH, r.t., 30 min. (87%); (h) DMFDMA, DMF, 80 °C. 1.5 h (43%) or iodopropane, NaH, DMF, 55°C, 30 min, (9%); (i) oxetan-3-amine, DIPEA, DMA, 100 °C, 18 h (100%); (j) trichloroisocyanuric acid, DBU, MeOH, r.t., 24 h. (19%); (k) MeI, TBAB, NaOH, DCM, water, r.t., 36 h, (92%); (l) boronic ester, dichloro [1,1'- bis(di-tertbutylphosphino)ferrocene] palladium(II), K_2CO_3, Dioxane, 80 °C, 1 h (58%); (m) 3-methoxycyclobutan-1-amine.HCl, DIPEA, DMA, 100°C, 16 h (68%); (n) trichloroisocyanuric acid, DBU, MeOH, r.t., 18 h. (99%); (o) MeI, TBAB, NaOH, DCM, water, r.t., 12 h, (75%); (p) arylboronate, Cs_2CO_3, $Pd(PPh_3)_4$, dioxane:water, 80-90 °C, 2-3 h (36-75%); (q) (6-fluoropyridin-3-yl)boronic acid , K_2CO_3, $Pd(PPh_3)_4$, dioxane:water, 90 °C, 4

h (86%); (r) alcohol, NaH, DMF or DMA, r.t., 10 min - 24 h (25-75%) (for **45** an additional step: TFA, DCM, r.t. 1 h, was required); (s) (6-(3-bromopropoxy)pyridin-3-yl)boronic ester, Cs_2CO_3, $Pd(PPh_3)_4$, dioxane:water, 90 °C, 1 h (27%); (t) MsCl, DIPEA, DMF, r.t., 30 min. (u) morpholine, DIPEA r.t, (9% over 2 steps).

Scheme 4:[a] Synthesis of 1H-imidazo[4,5-c]quinolin-2(3H)-ones by Curtius rearrangement.

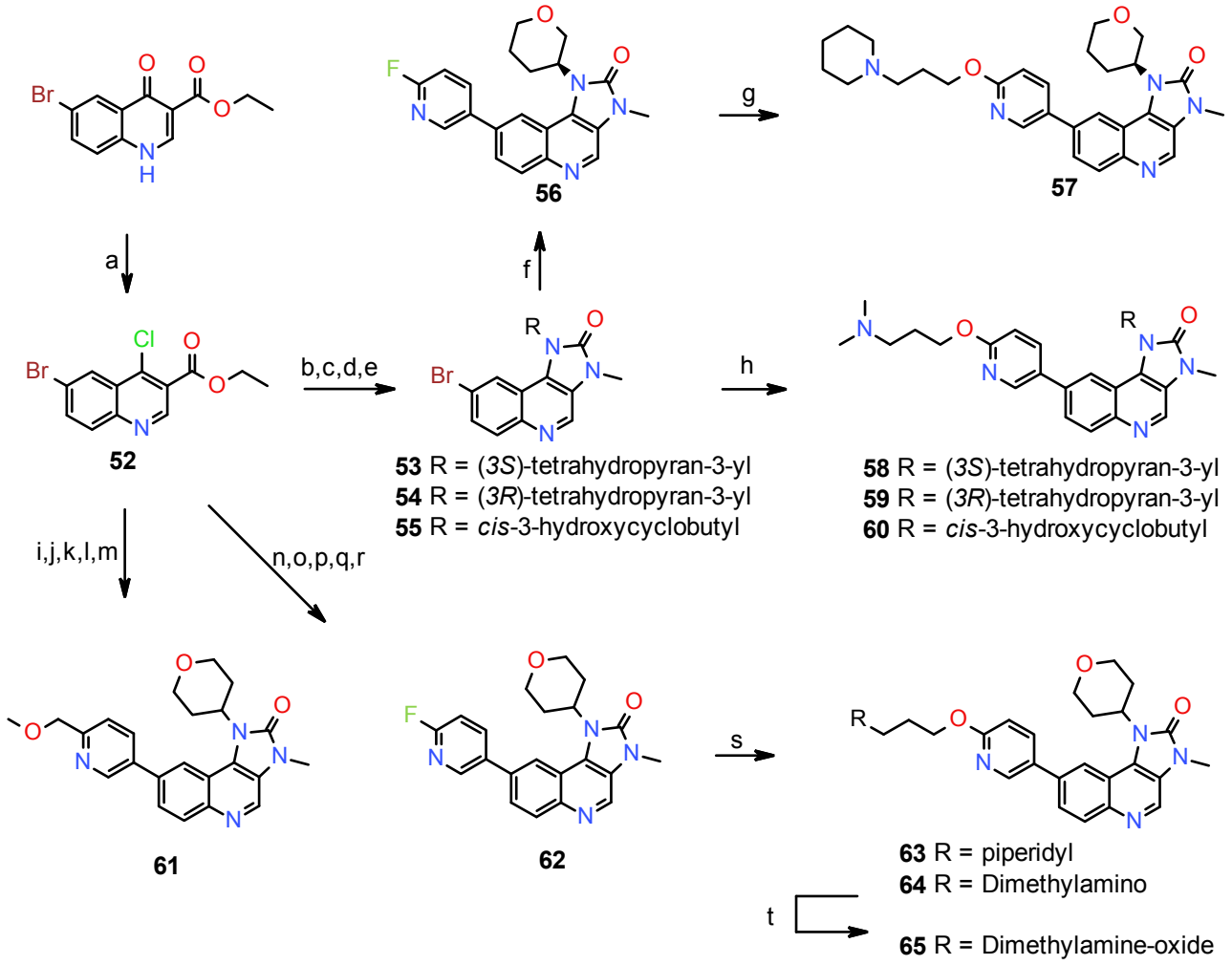

[a] Reagents and conditions: (a) $SOCl_2$, DMF, 75 °C, 16 h (83%); (b) amine, DIPEA, DMA, 80-90 °C, 1.5-16 h (83-97%); (c) NaOH, THF, MeOH, Water, 60 °C, 1.5-3 h (95-100%); (d) DPPA, TEA, DMF, 60 °C, 1-16 h, (80-98%); (e) MeI, TBAB, NaOH, DCM, water, r.t., 1-12h or DMFDMA, DMF, 80°C, 3h (75-96%); (f) (6-fluoropyridin-3-yl)boronic acid, Cs_2CO_3, $Pd(PPh_3)_4$, dioxane:water, 100 °C, 3 h (87%); (g) 3-(piperidin-1-yl)propan-1-ol, NaH, THF, r.t., 24 h (28%); (h) aryl boronic ester, Cs_2CO_3, X-phos-2Gen or $Pd(PPh_3)_4$, dioxane:water, 90-100 °C, 2-3 h (41-62%); (i) tetrahydro-2H-pyran-4-amine, DIPEA, DMF, 60 °C, 16h (100%);(j) 2-(methoxymethyl)-5 -boronic ester-pyridine Cs_2CO_3, $Pd(PPh_3)_4$, dioxane:water, 100 °C, 2 h (95%) ; (k) NaOH, THF, Water, 60 °C, 4 h (92%); (l) DPPA, TEA, DMF, 60 °C, 7 h, (79%); (m) MeI, TBAB,

NaOH, DCM, water, r.t., 72 h (62%); (n) tetrahydro-2H-pyran-4-amine, DIPEA, DMF, 60 °C, 16h (100%); (o) NaOH, MeOH, Water, 70 °C, 2 h (86%); (p) DPPA, TEA, DMF, 60 °C, 2 h, (99%); (q) MeI, TBAB, NaOH, DCM, water, r.t., 16 h (93%); (r) (6-fluoropyridin-3-yl)boronic acid, Cl_4Na_2Pd, DTBPPS, K_2CO_3, dioxane:water, 100 °C, 16 h (96%); (s) alcohol, NaH, DMA or DMF, r.t. to 50 °C, 2-16 h, (82-90%); (t) NADP, K_2PO_4, Codexis KRED, Codexis BVMO, 2-propanol, water, r.t., 41 h (39%).

Imidazo[4,5-c][1,5]naphthyridin-2-one **70** was synthesized in 8 steps from 6-chloro-3-aminopyridine **67**. Enamine formation followed by cyclisation and hydrolysis gave bicycle **68**. Chlorination and amide formation followed by S_NAr and Hoffman rearrangement led to intermediate **69** which was converted to **70** by methylation and finally Suzuki cross-coupling with the appropriate boronate, scheme 5.

Scheme 5:[a] Synthesis of **70**.

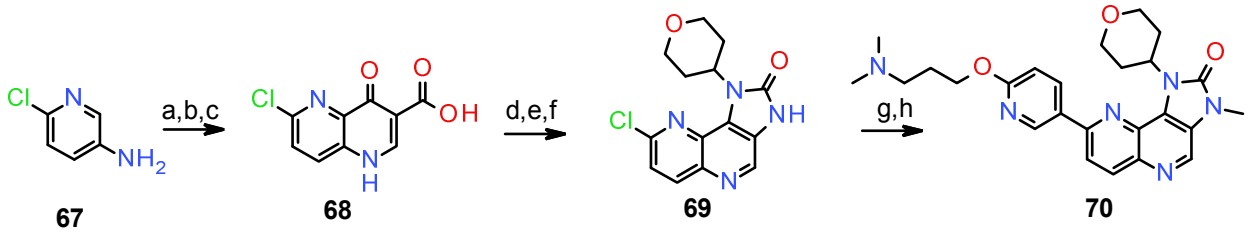

[a] Reagents and conditions: (a) 1,3-diethyl 2-(ethoxymethylidene)propanedioate, EtOH, 80 °C, 4 h (90%); (b) Ph_2O, 220 °C, 2 h (37%); (c) NaOH, EtOH, water, 100 °C, 0.5 h (92%); (d) $SOCl_2$, DMF, 80 °C, 2 h; NH_4OH (100%); (e) tetrahydro-2H-pyran-4-amine·HCl, DIPEA, DMA, r.t., 18 h (37%); (f) trichloroisocyanuric acid, DBU, MeOH, r.t., 30min. (75%); (g) MeI, TBAB, NaOH, DCM, water, r.t., 12 h (75%); (h) boronic ester, Cs_2CO_3, $Pd(PPh_3)_4$, dioxane:water, 90 °C, 2 h (28%).

Imidazo[4,5-c]cinnolin-2-one **74** was made in 10 steps from 4-bromophenylhydrazine **71**. Initial reaction with diethyloxomalonate was followed by hydrolysis of both esters and acid chloride formation. Titanium chloride induced cyclisation afforded cinnoline **72**. Chlorination, S_NAr, ester hydrolysis and Curtius rearrangement led to the formation of tricylcic compound **73** and methylation followed by a Suzuki cross-coupling produced **74**, scheme 6.

Scheme 6:[a] Synthesis of **74**

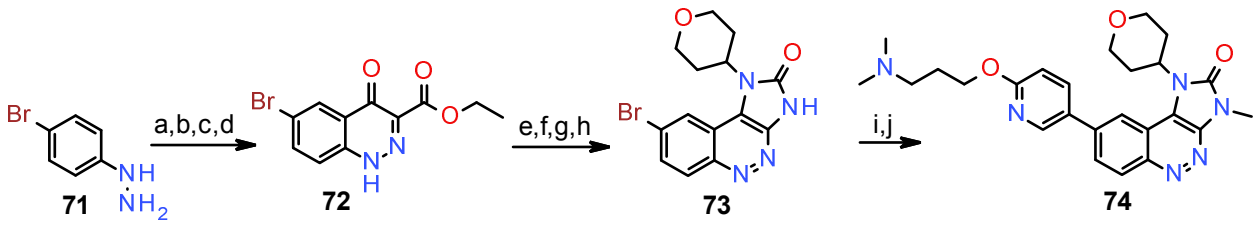

[a] Reagents and conditions: (a) Diethyloxomalonate, aq EtOH, r.t., 18 h (92%); (b) NaOH, EtOH, 78 °C, 50 min. (81%); (c) $SOCl_2$, 44°C, 2 h, (97%); (d) $TiCl_4$, nitrobenzene, 95 °C, 18 h then EtOH, H_2SO_4, 95 °C, 5 h (34%); (e) $SOCl_2$, 75°C, 3 h, (100%); (f) tetrahydro-2H-pyran-4-amine.HCl, TEA, THF, r.t., 30 min. (98%); (g) NaOH, MeOH, water, r.t., 1 h; (h) DPPA, TEA, DMF, 60 °C, 3 h (60% over 2 steps); (i) DMFDMA, DMF, 80 °C, 4 h (91%); (j) Boronic ester, Cs_2CO_3, $Pd(PPh_3)_4$, dioxane:water, 80 °C, 2 h (8.5%).

RESULTS AND DISCUSSION

A number of strategies for reducing the predicted clinically efficacious dose can be conceived; however, to identify the optimal strategy it is important to consider the extent to which different parameters contribute to the dose prediction. For example, increasing potency (whilst keeping all other parameters constant) will reduce the predicted dose in a linear fashion; however, increases in the pharmacokinetic half-life can have a much more profound influence (especially where the predicted half-life is significantly shorter than the desired duration of target engagement). Given the relatively short predicted human half-life of **7**, especially in the context of achieving target engagement for a 24 hour period, we embarked on a strategy to increase half-life whilst maintaining or improving potency, selectivity and physicochemical properties. The use of PBPK modelling approaches to accurately predict human pharmacokinetics requires detailed *in vitro* and *in vivo* compound profiling and as such places a limit on the number of compounds for which such models can be built. However, a reasonable first estimate of human pharmacokinetic parameters can be produced based on a more limited set of *in vitro* parameters (*i.e.* plasma protein binding and the intrinsic clearance in human hepatocytes)

combined with a prediction of the volume of distribution (V_{ss}). When combined with a knowledge of target potency and the required extent and duration of target engagement an estimate of clinical dose can be made. This simplified prediction, termed early dose to man prediction (eD2M) within AstraZeneca, assumes complete absorption of a compound across the gut (*i.e.* F_{abs} = 100%) which would only be expected to hold true for highly permeable compounds.[45] However, if available, V_{ss} and F_{abs} data determined experimentally in rodents can be incorporated to refine the prediction. The use of eD2M and D_{abs} predictions enables a comparison of compound quality across a large number of compounds and was used to guide the compound optimization described herein.

Pharmacokinetic half-life is intrinsically linked to both the clearance (CL) and the V_{ss} of a compound and both parameters were considered for optimization. Compound **7** displays low metabolic turnover in human hepatocyte incubations suggesting that a further reduction in CL would be a challenge; therefore, a strategy to increase V_{ss} was considered more profitable. Many studies have been reported attempting to identify those molecular properties that influence V_{ss} with ionization state often found to dominate.[46] In particular, basic compounds generally show increased V_{ss} when compared with neutral or acidic compounds thus suggesting that the incorporation of a basic substituent into our novel series of ATM inhibitors, whilst keeping other parameters constant, would deliver an increased predicted human half-life and reduced predicted clinical dose.

Figure 2: Structure of basic quinoline carboxamide **16**

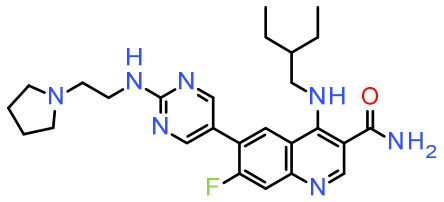

16

Wide ranging SAR exploration in the 6-position of the quinoline carboxamide scaffold revealed the potential to incorporate a basic substituent, as exemplified by **16**, figure 2. Compound **16** showed an unexpected increase in ATM cell potency (IC_{50} = 0.0086 μM) whilst selectivity over ATR was retained (IC_{50} >30 μM) and the basic nature of the compound resulted in an increased predicted human V_{ss} when compared to neutral compound **7** (3.5 L/kg *c.f.* 1.2 L/kg). The improved primary potency and increased V_{ss} of **16** culminated in a low predicted clinical efficacious dose (eD2M = 11 mg QD) thereby highlighting how optimization of primary potency and pharmacokinetic properties can influence the predicted dose. Unfortunately, despite this low dose prediction the permeability of the **16** was poor and a significant efflux liability was observed in MDCK cells (P_{app} A-B = 0.8 x 10^{-6} cm/s, efflux ratio = 28) suggesting that this compound is unlikely to have good oral bioavailability or F_{abs} and would, therefore, be unsuitable for further development. It should be noted that the anticipated poor F_{abs} of **16** will adversely affect the accuracy of the eD2M prediction. The poor permeability observed with a lipophilic compound such as **16** (log $D_{7.4}$ = 2.8) emphasizes the impact that ionization and hydrogen bonding groups (in particular donating groups) can have on permeability. Previously reported SAR studies have established the importance of the 4-amino and 3-carboxamide motifs within this scaffold culminating in the hypothesis that an internal hydrogen bond is formed between these motifs to organize the molecule into a bioactive conformation.[30] As a consequence, all attempts to reduce hydrogen bond donor count within this scaffold have been unsuccessful and it was, therefore, considered improbable that a permeable, basic compound could be delivered without increasing lipophilicity to an unacceptable level. Accordingly, it was appreciated that an inherently more permeable series of selective ATM inhibitors would be required to allow the continuation of our strategy to increase both primary potency and pharmacokinetic half-life through the introduction of basic substituents.

Numerous examples of chemical scaffold hopping exist in which a cyclic motif within a molecule is replaced with a "pseudo" ring system (constrained by an intramolecular hydrogen bond) leading to compounds with similar conformations and biological activities.[47] The presence of a

"pseudo" cyclic system within the quinoline carboxamide scaffold prompted the consideration of suitable cyclic systems which could replace this "pseudo" ring and retain the ability to correctly position any appended substituents. Such a strategy, if successful, was anticipated to maintain ATM potency and selectivity whilst reducing the number of hydrogen bond donors and increasing permeability. A number of possible tricyclic systems with the potential to fulfil the desired criteria were conceived but the imidazo[5,4-c]quinolin-2-one scaffold was prioritized based on in-house data on novel, proprietry AstraZeneca compounds that was generated during routine cross project selectivity screening. This data highlighted the potential for compounds based on this scaffold to display potent activity against a range of PIKK family members. It should be noted that a similar scaffold is also present in a dual PI3K / mTOR inhibitor, NVP-BEZ235, which has been reported as undergoing clinical evaluation; NVP-BEZ235 is reported to have activity against ATM.[48-50] Although this activity for NVP-BEZ235 was not appreciated at the time of the work described it further supports the proprietry AstrsaZeneca data supporting the potential of imidazo[5,4-c]quinolin-2-one containing compounds to deliver potent ATM inhibitors whilst also further highlighting the challenge to achieve PIKK family selectivity with such a scaffold. A comparison of **38** with **36** reveals that ATM potency is broadly maintained following the scaffold hop confirming that both cores can correctly position substituents in a bioactive conformation, table 2. However, selectivity against closely related kinases appeared reduced with **38** being more potent against ATR than against ATM. Permeability is increased, and efflux decreased, for **38** when compared to **36** despite the compounds possessing similar levels of lipophilicity supporting the importance of restricting hydrogen bond donors when optimizing permeability. Compound **38** retained good stability in hepatocyte incubations although aqueous solubility was reduced. Further investigation of the imidazo[5,4-c]quinolin-2-one demonstrated that the removal of a methyl group to deliver **37** was broadly tolerated, although the addition of a hydrogen bond donor may be expected to reduce permeability. Replacing the methyl with a larger substituent, **39**, resulted in the loss of activity against both ATM and ATR suggesting that there is little opportunity to increase primary potency or selectivity in this region of the molecule.

Table 2: Structures and profiles of **36** – **39**.[a]

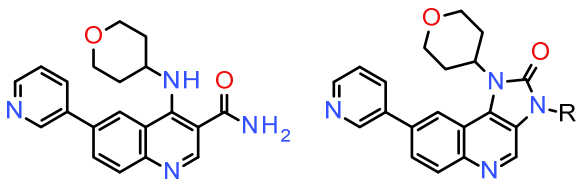

36

38 R = Me
37 R = H
39 R = ^{i}Pr

	36	**38**	**37**	**39**
ATM Cell IC_{50}	0.95	0.36	1.6	>30
ATR Cell IC_{50}	3.1	0.087	0.051	>27.6
Log$D_{7.4}$	1.9	2.2	2.4	2.9
Aqueous Solubility	>610	17	12	41
Human / Rat Heps	<4 / 8.5	<4.9 / 9.4	-	-
hERG IC_{50}	2.1	11	-	-
MDCK P_{app} A-B / efflux ratio[b]	4.8 / 10	30 / 1.5	-	-
Caco2 P_{app} A-B / efflux ratio[b]	15 / 4.5	60 / 0.6	-	-

[a] Data reported as in table 1.

[b] P_{app} A-B data are expressed in 10^{-6} cm/s and the efflux ratio is expressed as P_{app} B-A / P_{app} A-B

In order to better understand how these compounds bind to ATM an *in silico* model of the protein was built using the MOE/2014 software (Chemical Computing Group) and the structure of related protein kinase mTOR as a template (PDB code = 4JSX). Alignment was performed based on sequence similarity and conserved features of protein kinases. Ten candidate homology models of ATM were built, retaining the original mTOR ligand to prevent collapse of the binding site and the best model in terms of protein structure quality criteria was selected and further refined. Standard procedures as outlined in the MOE documentation were employed throughout. Example ligands were docked into the binding site using the default docking algorithm in MOE and twenty poses were kept for each with the best pose selected manually, based on SAR knowledge. When modelled into the ATP-binding site of

ATM both **36** and **38** showed highly similar binding modes in which the molecules were anchored through a hydrogen-bond from the quinoline nitrogen to Cys2770 in the hinge region of the kinase, figure 3. A second hydrogen-bond was formed from the pyridine ring to the conserved catalytic lysine (Lys2717), while the same ring bypasses the gatekeeper residue (Leu2767) to take part in an edge-face π- interaction with Tyr2755, within the back pocket. In order to make these interactions the pyridine ring is twisted ~35° out of the plane of the quinoline ring. These predicted interactions are consistent with the observed activities. The postulated internal hydrogen bond was predicted for **36** and is again consistent with the observed SAR. The tetrahydropyran group was not predicted to make any specific interaction and was predicted to partly occupy the ribose binding pocket

Figure 3a: *In silico* model of ATM with **36** bound into the ATP binding site.

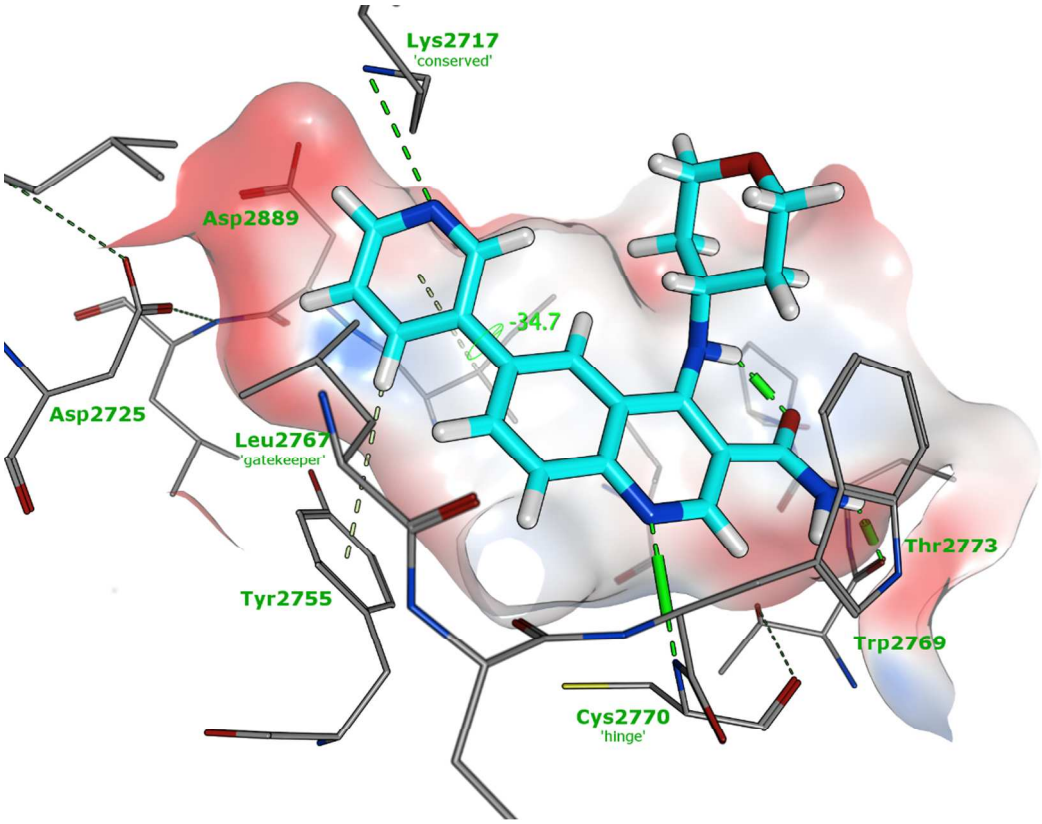

Figure 3b: *In silico* model of ATM with **38** bound into the ATP binding site.

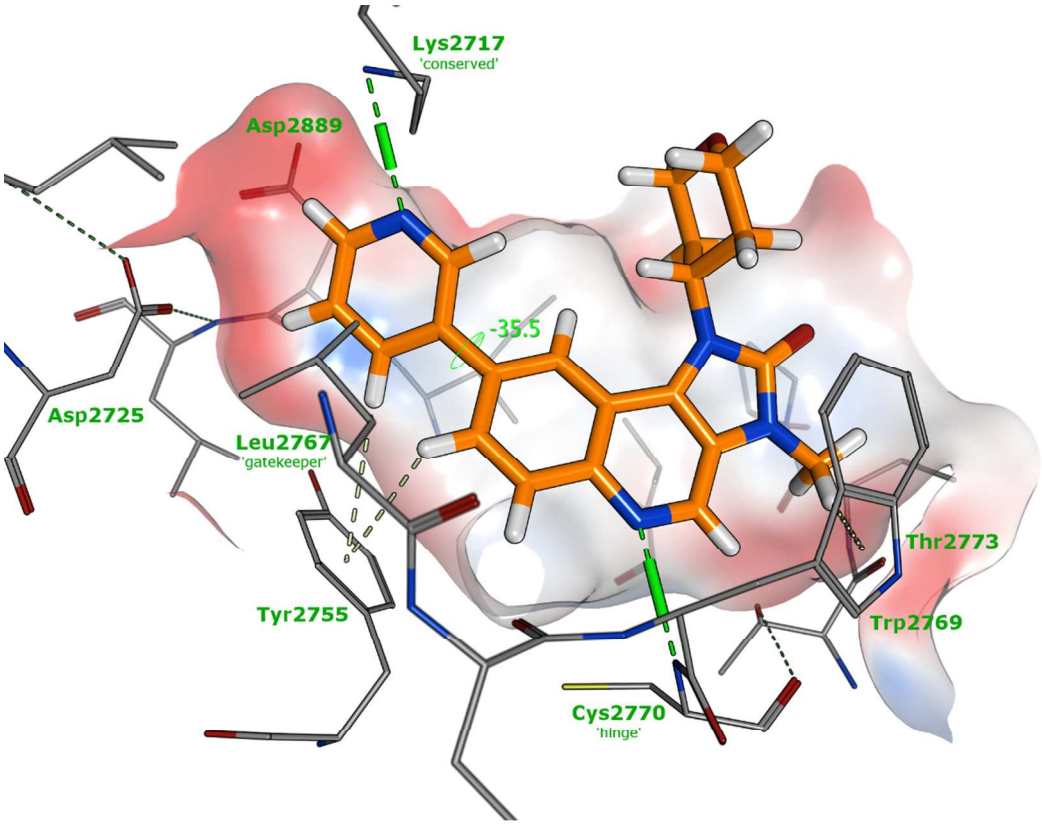

To further probe the hypothesized binding modes the methoxymethylpyridine motif, present in both **6** and **7** and known to increase selectivity for ATM over ATR in the quinoline carboxamide scaffold, was incorporated into the imidazo[5,4-c]quinolin-2-one scaffold to produce **61**, table 3. Encouragingly, **61** retained activity against ATM whilst activity against ATR was dramatically reduced thereby restoring the desired selectivity profile. Compound **61** was highly permeable and stable in human hepatocyte incubations although aqueous solubility was low. The incorporation of a fluorine in the 7-position of the imidazo[5,4-c]quinolin-2-one core, **18**, was found to improve solubility and reduce metabolic turnover in rat hepatocyte incubations, albeit ATM potency was slightly diminished. Chloro- and methoxy-substituents were also tolerated in this position, albeit with a 3-10 fold reduction in ATM potency (data not shown). This SAR is analogous to that observed with the quinoline carboxamide scaffold further supporting the modelled binding modes. Based on the quinoline carboxamide SAR, larger substituents in this position would not be expected to have good affinity for ATM and hence no further investigation was performed. Interestingly, the impact of the fluorine on hERG affinity appears

less marked in the imidazo[5,4-c]quinolin-2-one scaffold. Divergent SAR between the two series was observed when replacing the tetrahydropyran motif where the introduction of a previously optimized chiral amine to the imidazo[5,4-c]quinolin-2-one scaffold, **20**, failed to deliver the anticipated increase in potency. This observation suggests that the positioning of this substituent differs slightly between the two scaffolds which is also consistent with the proposed binding modes. More thorough evaluation of the SAR in this region uncovered a number of small cyclic alkyl groups with improved ATM potency, good selectivity and high levels of permeability, for example **12** – **15**, table 3. The addition of a hydrogen bond donor in this region did result in a reduction in permeability, **15**, albeit the overall profile remained encouraging. Pharmacokinetic evaluation of **13** in rat revealed the compound to have good bioavailability (>100%) and moderate CL (22.5 mL/min/kg). However, as anticipated for a neutral compound, V_{ss} was relatively low (0.98 L/kg) leading to a modest half-life (2.7 h). The properties of **13** resulted in a large predicted clinically efficacious dose (eD2M >10000 mg QD) and thus highlighted that although the imidazo[5,4-c]quinolin-2-one scaffold had the potential to deliver selective ATM inhibitors, significant optimization of both primary potency and predicted human pharmacokinetics was required.

Table 3: SAR exploration of neutral imidazo[5,4-c]quinolin-2-ones.[a]

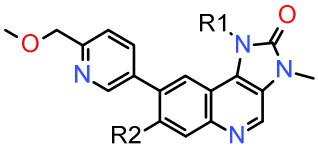

Entry	R1	R2	ATM Cell IC_{50}	ATR Cell IC_{50}	Log$D_{7.4}$	Aq Sol	human / rat heps	hERG IC_{50}	P_{app} A-B / Efflux ratio
61		H	0.37	>13	2.3	19	<3 / 63	>33	32 / 1.4
18		F	0.45	>20	2.4	99	<4 / 7.5	27	43 / 0.8
20	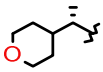	F	0.49	>30	2.7	>1000	22 / 1.6	15	27 / 0.8

12	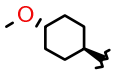	F	0.24	>26	3.2	84	10 / 10	27	20 / 0.6
13	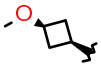	F	0.10	>30	2.7	37	8.8 / 4.5	9.0	38 / 0.4
14	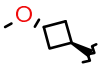	F	0.16	>28	3.0	49	8.4 / 4.3	8.9	28 / 0.6
15	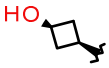	F	0.14	>30	2.0	270	2.7 / 6.0	15	14 / 2.6

[a] Data reported as in table 1 and table 2.

With an understanding of how the two series bind we were able to use our detailed knowledge of the quinoline carboxamide SAR to inform the design of compounds **29**, **30** and **24**, table 4. Consistent with the quinoline carboxamide SAR, the methoxy motif could be replaced by hydroxyl (**29**) or methylsulfonyl (**30**) leading to reduced lipophilicity with only limited impact on ATM potency; however, permeability was compromised to some extent and solubility remained low. The introduction of a basic substituent (**24**) resulted in a significant increase in ATM potency and solubility and whilst permeability was compromised the profile was considered superior to that for basic quinoline carboxamide compound **16**. The concept of Lipophilic Ligand Efficiency (LLE) has been widely reported in the literature and is routinely used within the Medicinal Chemistry community as a measure of compound quality.[51,52] When comparing the LLE (ATM Cell $pIC_{50} - \log D_{7.4}$) of **13** and **24** a clear improvement was observed (LLE = 4.3 and 6.5 respectively) indicating the advantageous nature of the basic side chain. This advantage is more apparent when comparing the predicted clinically efficacious clinical dose (**24**: eD2M = 24 mg QD) and was further validation for our focus on primary potency and predicted human pharmacokinetics. The low predicted clinically efficacious dose for **24** prompted the more thorough exploration of basic substituents with a focus on improving permeability whilst maintaining or increasing ATM potency. Removal of the hydrogen bond donor by methylation of the nitrogen, **25**, did increase permeability although a reduction in potency was observed, table 4. Replacing the nitrogen with oxygen, **31**, was also found to increase permeability and the impact on ATM potency was much diminished resulting in a more attractive balance of properties. Amidic linker groups were

also investigated, **27** and **28**, but no improvement in permeability was observed. The high potency of **28** implied that longer basic chains could be accommodated and it was quickly established that a three carbon chain, linked to the pyridine through an oxygen atom (**32**), was optimal. Compound **32** was a highly potent and selective ATM inhibitor with excellent solubility, reasonable hepatic stability and no activity against hERG. The increased basicity of **32** compared to **31** (pK_a = 9.3 and 8.5, respectively) led to a reduction in Log$D_{7.4}$ and whilst a slight reduction in permeability was observed the profile remained highly attractive. The dramatic improvement in ATM potency for **32** compared to neutral compound **13**, alongside the increased predicted V_{ss} associated with a basic group (predicted human V_{ss} = 2.7 L/kg), culminated in a >1000-fold reduction in predicted clinically efficacious dose (**32**: eD2M = 16 mg QD).

Table 4: Structure and profile of compounds **24**, **25**, **27**, **28**, **31**, and **32**.[a]

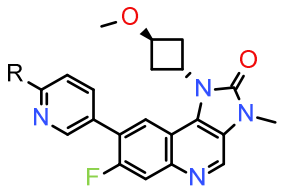

Entry	R	ATM Cell IC_{50}	ATR Cell IC_{50}	Log$D_{7.4}$	Aq Sol	human / rat heps	hERG IC_{50}	P_{app} A-B / Efflux ratio
29		0.23	15	2.0	23	- / 5.0	23	29 / 1.1
30		0.16	>16	1.3	18	- / 2.4	14	14 / 2.4
24	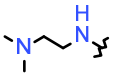	0.006	>30	1.7	>1000	2.8 / 9.6	24	3.4 / 11
25	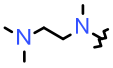	0.23	>30	2.2	>1000	5.1 / 18	5.7	6.3 / 3.5
27	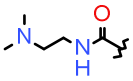	0.13	>30	1.5	980	4.0 / 2.9	>33	2.5 / 11

28	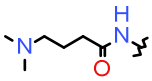	0.0082	>30	1.1	870	6.5 / 7.0	18	0.4 / 77
31	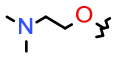	0.023	>30	2.0	>1000	8.3 / 12	>33	16 / 1.6
32	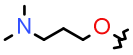	0.0011	>30	1.8	>980	7.9 / 6.6	>33	6.8 / 6.2

[a] Data reported as in table 1 and table 2.

The positive impact of the basic substituent on both aqueous solubility and hERG affinity prompted the re-evaluation of the 7-fluoro substituent. Removal of the fluorine, **42**, delivered a further increase in ATM potency with little affect on other properties, table 5. Interestingly, incorporation of the fluorine substituent on the pyridyl ring, **43**, resulted ATM potency similar to **32**, whilst the inclusion of two fluorine atoms, **33**, gave a minor reduction in potency. This pattern of activity was seen across a range of fluorinated and non-fluorinated matched sets (data not shown) and a possible explanation for this could involve the preferred conformation of the biaryl bond linking the pyridyl ring to the imidazo[5,4-c]quinolin-2-one core. The proposed binding mode contains a dihedral angle of ~35° allowing a π-interaction between a ring hydrogen and Tyr2755 of the protein. Quantum mechanics calculations (DFT, B3LYP, 6-31G**) of this biaryl system confirm the binding mode prediction that a non-planar conformation is preferred and the variation in conformational strain as a function of dihedral angle is shown in figure 4. When no fluorine atoms are present (*e.g.* **42**) the energy minimum sits at 36°, while a fluorine at the 7-position of the core (*e.g.* **32**) increases the dihedral of the lowest energy conformation to 41°. The energy penalty incurred for fluorinated analogues to adopt the preferred binding conformation is consistent with the subtle reduction in potency observed. This hypothesis is also consistent with the observed SAR for the introduction of a chloro- or methoxy-substituent in this region.

Table 5: Structure and profile of compounds **42**, **43** and **33**.[a]

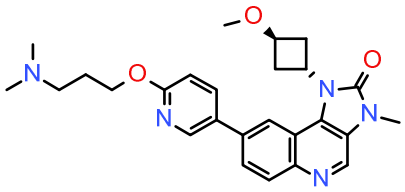

42

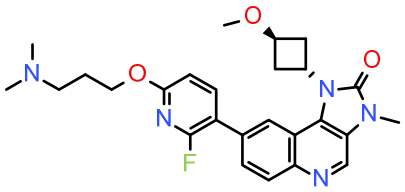

43

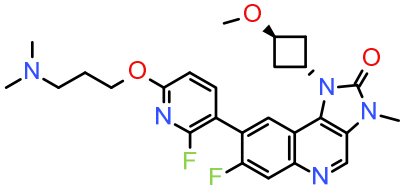

33

Entry	ATM Cell IC_{50}	ATR Cell IC_{50}	Log$D_{7.4}$	Aq Sol	human / rat heps	hERG IC_{50}	P_{app} A-B / Efflux ratio
42	0.00025	>30	1.6	540	8.7 / 5.1	>33	7.8 / 3.0
43	0.00076	>30	2.0	>1100	15 / 9.3	>33	4.2 / 3.2
33	0.0026	>30	2.1	>1000	14 / 9.0	22	10 / 2.5

[a] Data reported as in table 1 and table 2.

Figure 4: Relative energy for the conformational strain of a biaryl system as a function of dihedral with different substitution patterns, from quantum mechanics (DFT, B3LYP, 6-31G**).

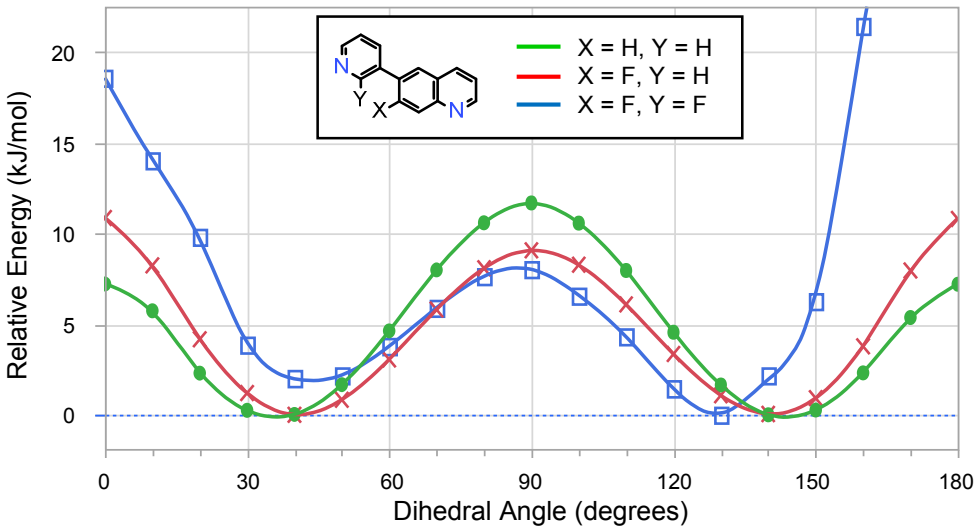

Pharmacokinetic evaluation of **42** in both rat and dog revealed moderate clearance (19.5 and 27.6 mL/min/kg, respectively) but the relatively high V_{ss} (5.7 and 11 L/kg, respectively), driven by the basic

nature of the compound (pK_a = 9.5), resulted in a half-life of approximately 5 hours in both species. The permeable nature of **42** led to good bioavailability in both rat and dog (50% and 65%, respectively). PBPK modelling suggested that **42** would have a moderate to high clearance in humans (~13 mL/min/kg) but that a high V_{ss} (>10 L/kg) would produce a long half-life (~15 hours). The predicted clinically efficacious dose was estimated to be 3 mg QD with a free C_{max} in the region of 0.001 μM. GI-Sim modelling predicted the D_{abs} for **42** would to be 3500 mg, thereby suggesting that compound **42** could be well suited for clinical development. However, the moderate to high predicted human clearance of **42** was considered to consitute a risk for lower than desired bioavailability in man, due to high first pass metabolism, especially when you consider the errors associated with predicted values. Therefore, despite the highly promising nature of **42** we believed there remained an opportunity for further compound optimization and in particular we sought to investigate the potential impact of cytochrome P450 mediated oxidative demethylation of the basic center. The methylamino analogue **45**, a potential product of such oxidative metabolism, was found to retain excellent potency and selectivity for ATM, table 6. As a consequence of the removal of a lipophilic methyl group, combined with the increased basicity of the compound (pK_a = 10.3), the Log$D_{7.4}$ is dramatically reduced and this, in conjunction with an increase in H-bond donnor count, results in compromised permeability. The incorporation of cyclic bases, **46** – **48**, was well tolerated and moderate improvements in metabolic stability were observed. However, detailed *in vitro* metabolite ID studies for **42** highlighted that oxidative dealkylation of the base was not the major metabolic pathway. Similar studies for **45** suggested that the cyclic base has the potential to undergo oxidative ring opening giving rise to potentially reactive species. Surprisingly, the morpholine containing and hydroxypiperidine containing compounds, **50** and **51**, have lost much of their affinity for ATM. It is currently unclear whether this was driven by a reduction in basicity (pK_a = 6.7 and 8.4, respectively) or the inability of the protein to accommodate hydrophilic atoms in that region.

Table 6: Structure and profile of compounds **45** – **48**, **51** and **52**.[a]

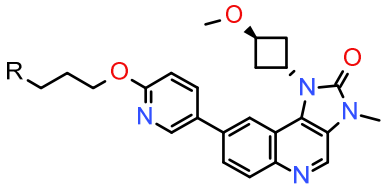

Entry	R	ATM Cell IC_{50}	ATR Cell IC_{50}	Log$D_{7.4}$	Aq Sol	human / rat heps	hERG IC_{50}	P_{app} A-B / Efflux ratio
45		0.00025	4.4	0.4	930	4.4 / 4.8	>33	0.65 / 41
46		0.00029	>24	1.4	770	3.3 / 2.5	>33	3.5 / 7.8
47		0.00017	>24	1.8	>1100	5.3 / <1.3	>33	2.5 / 9.4
48		0.00020	>2.6	2.2	>1000	3.0 / 4.0	14	5.4 / 1.9
50		>28	>30	1.4	980	- / 28	-	-
51		27	>30	0.6	750	- / <1	-	-

[a] Data reported as in table 1 and table 2.

To further enhance our understanding of the SAR we were keen to establish whether observations in different regions were independent of each other (*i.e.* additive SAR). Such knowledge was anticipated to help inform future compound design. A Free-Wilson type regression model, in which specific values are attached to individual structural motifs, was built using available data for the ATM cell pIC_{50} and found to predict well (RMSE <0.3) suggesting that the SAR is broadly additive in nature.[53] The use of such models has been employed by a number of groups to efficiency explore chemical space by helping to identify the combination of substituents most likely to result in a desired profile.[54-57] A similar strategy was adopted in which virtual compounds containing all possible combinations of tolerated substituents were prioritized for synthesis based on the likelihood of

possessing high ATM potency and falling within a desired lipophilicity range (predicted Log$D_{7.4}$ between 1.0 and 2.5). This strategy produced a number of highly potent compounds with good selectivity and physicochemical properties, exemplified by compounds in table 7, and **64** was identified as having a particularly attractive balance of properties. Whilst the tight control of lipophilicity and hydrogen bond donor count delivered compounds with generally acceptable levels of permeability, where these controls were not rigidly applied (or the predicted properties proved less accurate) compromised permeability could be observed, for example **40** and **60**. Although aqueous solubility remained high across the range of lipophilicity examined a trend of reduced solubility with increasing lipophilicity was observed, for example **63** and **57**.

Table 7: Structure and profile of compounds **35** – **42**.[a]

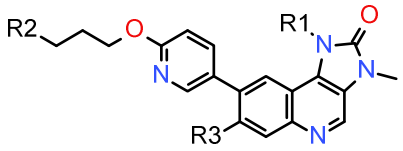

Entry	R1	R2	R3	ATM Cell IC_{50}	ATR Cell IC_{50}	Log$D_{7.4}$	Aq Sol	human / rat heps	hERG IC_{50}	P_{app} A-B / Efflux ratio
40			H	0.0015	>30	0.7	52	<1 / 7.8	>33	3.2 / 9.8
60	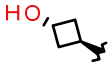		H	0.00024	>30	1.1	>1000	3.5 / 2.7	>33	<0.2 / >100
64			H	0.00057	6.2	1.5	>800	3.3 / 5.7	>33	6.6 / 5.1
19			F	0.00078	>30	1.5	>1000	6.8 / 8.3	>33	7.9 / 4.4
58			H	0.00033	>30	1.8	>1000	6.1 / 3.0	27	6.5 / 3.3
59			H	0.00094	>23	1.8	>1000	5.6 / 3.7	>33	7.5 / 2.1
63			H	0.0012	>29	2.1	310	5.3 / 5.1	>33	6.4 / 2.2
57			H	0.0011	>30	2.4	330	4.0 / 6.2	18	7.1 / 1.4

[a] Data reported as in table 1 and table 2.

Following thorough examination of the substitution around the imidazo[5,4-c]quinolin-2-one core attention was focused on changes to this core. In particular, the introduction of an additional heteroatom to produce imidazo[4,5-c][1,5]naphthyridin-2-one and imidazo[4,5-c]cinnolin-2-one containing compounds was explored, figure 5. Compounds based on the imidazo[4,5-c][1,5]naphthyridin-2-one scaffold, such as **70**, were found to broadly maintain potency against ATM but generally showed increased activity against ATR (**70**: ATM IC_{50} = 0.0017 μM, ATR IC_{50} = 2.0 μM) when compared to analogous compounds from the imidazo[5,4-c]quinolin-2-one scaffold. Increased lipophilicity and hepatic turnover were also observed for this scaffold (**70**: Log$D_{7.4}$ = 1.6; rat hepatocyte CL_{int} = 9.2 μL/min/10^6 cells, human hepatocyte CL_{int} = 12.8 μL/min/10^6 cells). Compounds based on the imidazo[4,5-c]cinnolin-2-one scaffold, such as **74**, showed reduced potency against ATM although selectivity over ATR was retained (**74**: ATM IC_{50} = 0.022 μM, ATR IC_{50} >30 μM). A reduction in lipophilicity was observed and compounds generally showed good hepatic stability (**74**: Log$D_{7.4}$ = 0.8; rat hepatocyte CL_{int} = 2.5 μL/min/10^6 cells, human hepatocyte CL_{int} <1 μL/min/10^6 cells). Whilst these data demonstrate that high quality imidazo[4,5-c][1,5]naphthyridin-2-one or the imidazo[4,5-c]cinnolin-2-one containing ATM inhibitors could be identified, based on the initial profiling none of the compounds characterized were considered to have a more attractive balance of properties than **64**.

Figure 5: Structures of **70** and **74**.

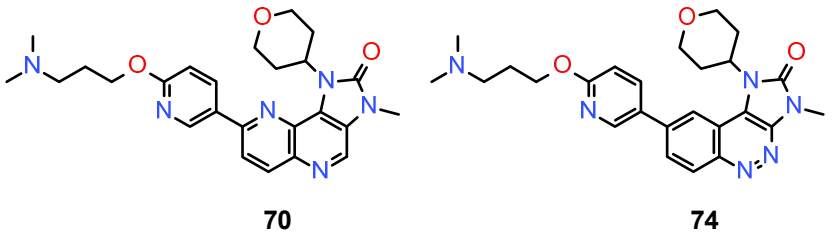

Detailed profiling of **64** revealed exceptional affinity to ATM enzyme and excellent selectivity over closely related targets in a range of available enzyme and cell assays, table 8. In addition, excellent general kinome selectivity was observed with only 2 kinases out of a panel of 397 showing >70% inhibition when screened at 1 μM (mTOR: 93%, LRRK2: 87%, see supporting information). Slurry experiments were used to identify the stable crystalline form for **64** and this was shown to have high levels of solubility in biorelevant media such as phosphate buffer at pH6.5, Simulated Gastric Fluid (SGF) and Fasted State Simulated Intestinal Fluid (FaSSIF), table 9. Compound **64** showed good levels of unbound drug in rat, dog and human plasma, reasonable permeability and did not inhibit any of the five major isoforms of human cytochrome P450 at concentrations up to 30 μM. Pharmacokinetic evaluation of **64** in both rat and dog show the compound has low to moderate clearance, moderate to high V_{ss} and good bioavailability, table 9.

Table 8: Selectivity profile of **64**

Target	Enzyme IC_{50} (μM)	Cell IC_{50} (μM)
ATM	0.00004*	0.00057
ATR	-	6.2
DNA-PK	0.14	-
mTOR	0.20	0.61
PI3Kα	0.32	1.4
PI3Kβ	1.8	-
PI3Kγ	1.1	-
PI3Kδ	0.27	-

* IC_{50} estimated following correction for tight binding based on the Morrison equation (Equation 9.6 in R.A. Copeland, *Enzymes*, 2nd edition, Wiley, 2000)

Table 9: Physicochemical and preclinical pharmacokinetic properties of **64**.

	64
pK_a	9.6

Solubility (pH6.5 / SGF / FaSSIF)	>5 mg/mL in all media
% free (rat, dog, human)	11%, 41%, 29%
MDCK P_{app} A-B / efflux ratio	6.6 x 10^{-6} cm.s^{-1} / 5.1
Caco2 P_{app} A-B / efflux ratio	5.6 x 10^{-6} cm.s^{-1} / 8.5
Caco2 P_{app} A-B @ pH6.5	19 x 10^{-6} cm.s^{-1}
Hepatocyte CL_{int} (rat, dog, human)	3.3, 3.3, 5.7, µL/min/10^6 cells
Rat PK (CL, V_{ss}, $T_{1/2}$, F)	15.5 mL/min/kg, 4.3 L/kg, 4.4 h, 57%
Dog PK (CL, V_{ss}, $T_{1/2}$, F)	33.3 mL/min/kg, 17.6 L/kg, 7.6 h, 54%
CYP inhibition (3A4, 2D6, 2C9, 1A2, 2C19)	IC_{50} >30 µM

The predicted binding mode of **64** highlighted the good complementarity of the molecule with the ATP binding site of ATM and predicted the same interactions with the kinase hinge (Cys2770), catalytic lysine (Lys2717) and back pocket (Tyr2755) that were present with **38**, figure 6a. In addition to this, the basic amine is predicted to sit in a highly polar subpocket, beyond the back-pocket, surrounded on three sides by the acidic residues Asp2725, Asp2720 and Asp2889. The interaction of the basic amine with these acidic residues is consistent with the observed increase in activity following optimization of the basic chain. In addition to understanding the likely bioactive conformation it is often informative to understand the unbound conformation of a molecule and assess how they differ. To this end we employed NMR techniques to determine accurately the unbound conformations of **64** and their dynamic motion in a physiologically-relevant solvent.[58] These studies concluded that the tetrahydropyran ring existed in a chair conformation with two distinct orientations: the major population of conformers (~60%) has the axial 4-hydrogen in directed away from the carbonyl group, the minor population (~40%) has the same hydrogen directed towards the carbonyl, figure 6b. The solution conformation also confirmed the anticipated twist between the pyridyl ring and the core and highlighted the rigid nature of the core. The conformation of the basic chain could not be determined indicating that there is free rotation in this region. The high degree of similarity between the solution conformation and the predicted bioactive conformation is likely to explain the exceptional level of affinity observed for **64** and closely related molecules.

Figure 6a: Predicted binding mode of **64** in ATM

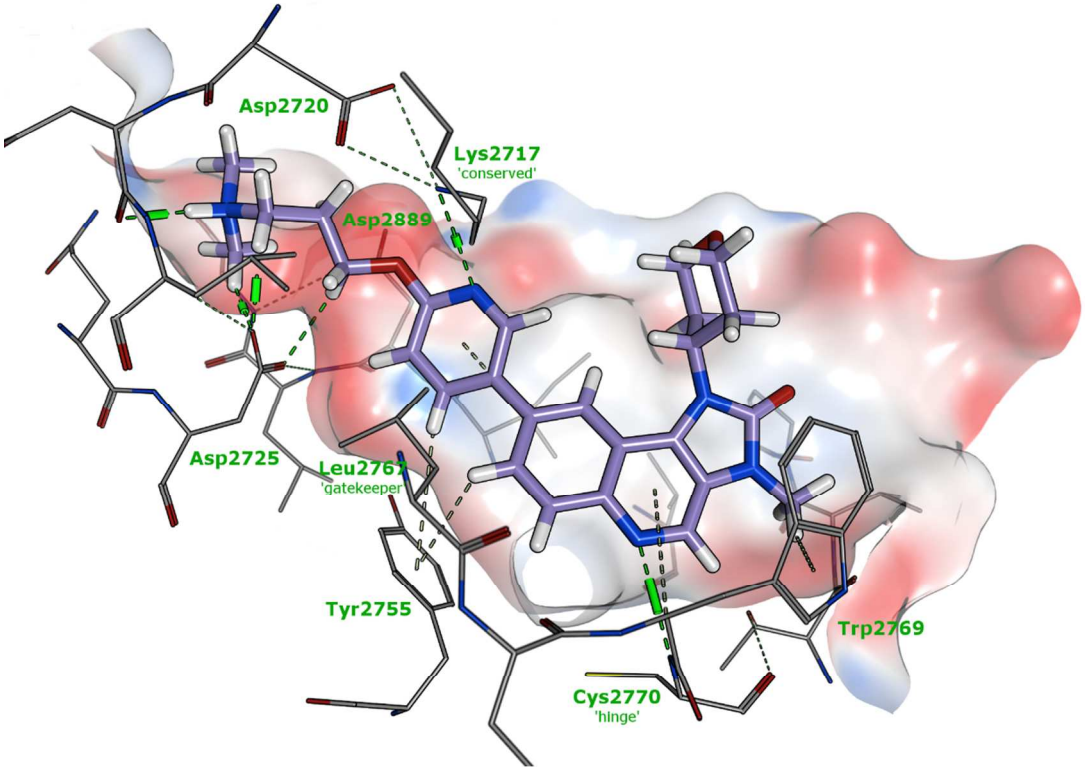

Figure 6b: Solution conformation of **64** as determined by NMR (major isomer in green, minor isomer in grey)

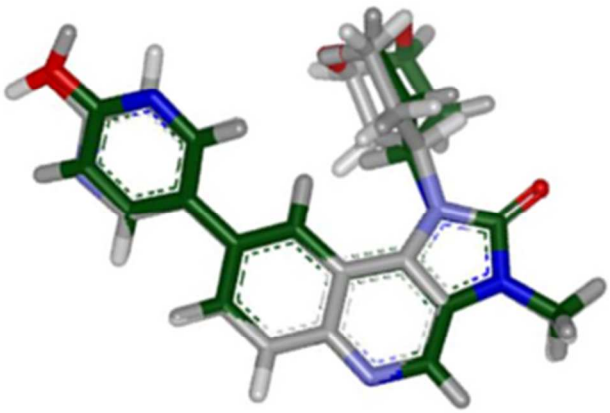

A detailed description of the *in vitro* and *in vivo* pharmacology of compound **64** is described elsewhere,[59,60] but the following data is included to exemplify the potential of **64** as an oral therapeutic agent. Compound **64** shows good exposure in mice following oral administration and its ability to potentiate the efficacy of DNA DSB inducing agents was assessed by combining with both irinotecan and olaparib.[61] A combination of irinotecan dosed at 50 mg/kg IP Q7D with **64** dosed orally at 20 mg/kg QD (on days 2-4 of a weekly cycle) was tolerated and caused tumor regression in an SW620 xenograft model in immunocompromised mice, thereby showing a clear potentiation of irinotecan monotherapy efficacy in this model, figure 7a. No appreciable efficacy was observed in this model when **64** was dosed as a monotherapy. The combination of **64**, dosed orally at 5 mg/kg QD (on days 1-3 of a weekly cycle), with olaparib, dosed orally at 50 mg/kg QD, was tolerated and caused tumor regression in immunocompromised mice bearing HBCx-10 patient derived tumors, thereby showing a clear potentiation of olaparib monotherapy efficacy in this model, figure 7b. HBCx-10 is a ductal adenocarcinoma with mutated Brca2, mutated TP53, no HER2 overexpression and no PR/ERα overexpression (*i.e.* it is triple-negative) which is sensitive to monotherapy treatment with olaparib when used as a mouse xenograft model.[62] Examination of the tumor growth in individual animals on this study showed that the efficacy of olaparib as a monotherapy in this model is variable with only 4 out of 10 mice treated showing tumor regression, figure 7c. However, when combined with **64** the response to olaparib was considerably improved with 9 out of 10 mice treated showing tumor regression, figure 7d. These *in vivo* studies clearly validate the ability of ATM inhibition to potentiate the efficacy of DNA DSB inducing therapies and supported the clinical evaluation of ATM inhibition as a novel mechanism to improve the efficacy of existing cancer therapies.

Figure 7a: 64 potentiates the efficacy of irinotecan in an SW620 xenograft model.

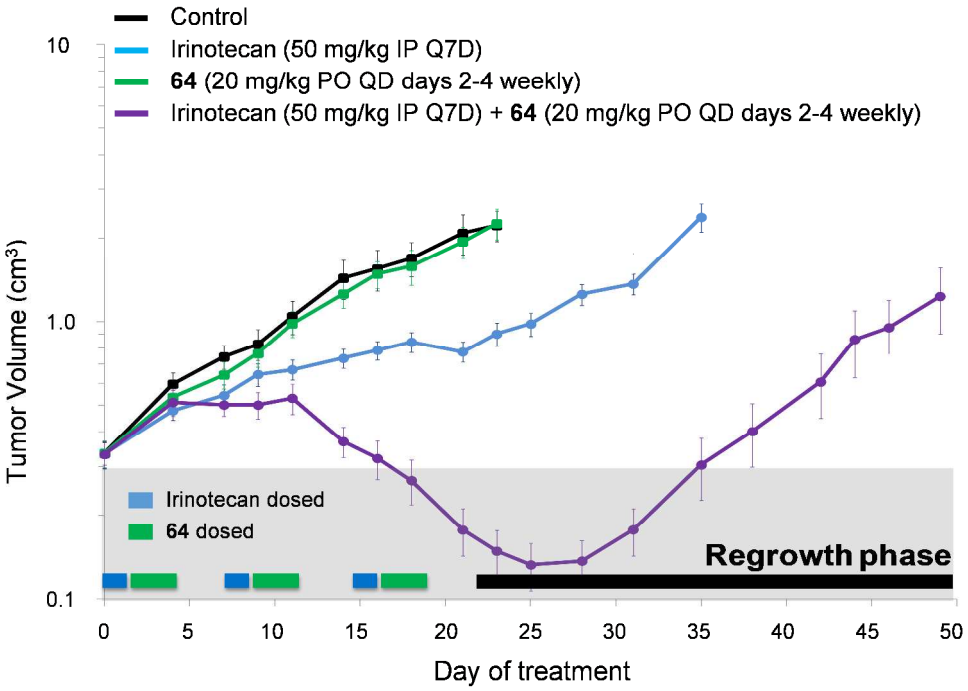

Figure 7b: 64 potentiates the efficacy of olaparib in a HBCx-10 patient derived tumor xenograft model.

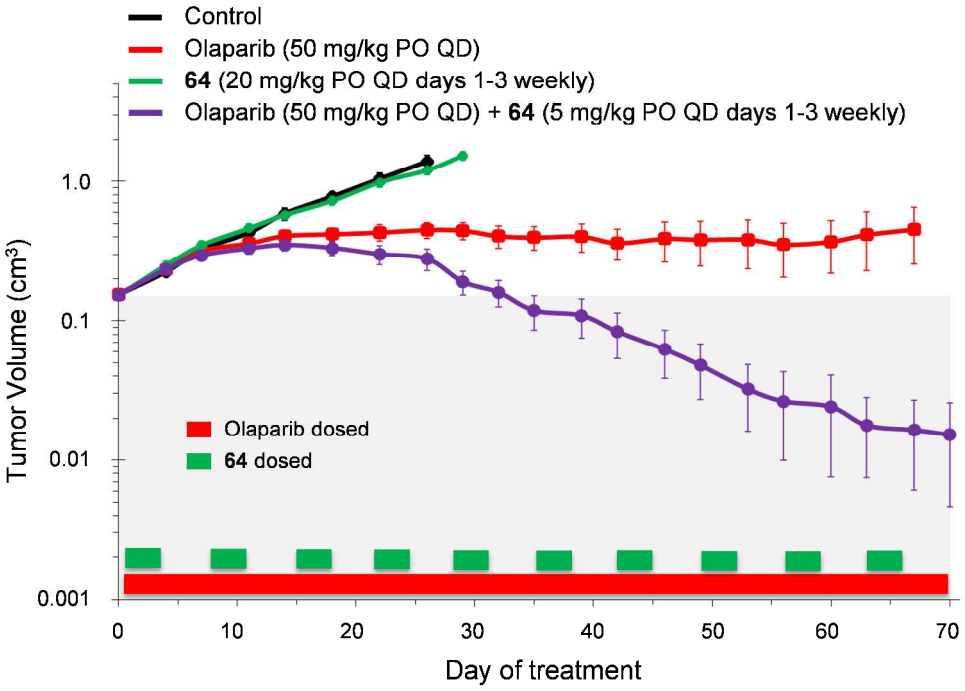

Figure 7c: 4 out of 10 mice show tumor regressions in a HBCx-10 patient derived tumor xenograft model following treatment with olaparib (50 mg/kg PO QD).

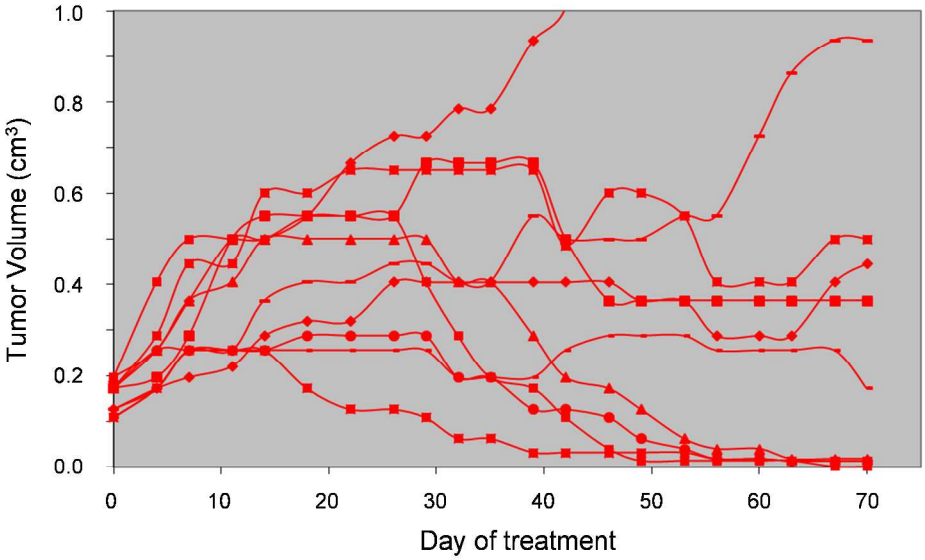

Figure 7d: 9 out of 10 mice show tumor regressions in a HBCx-10 patient derived tumor xenograft model following treatment with olaparib (50 mg/kg PO QD) and **64** (5 mg/kg PO QD days 1-3 weekly).

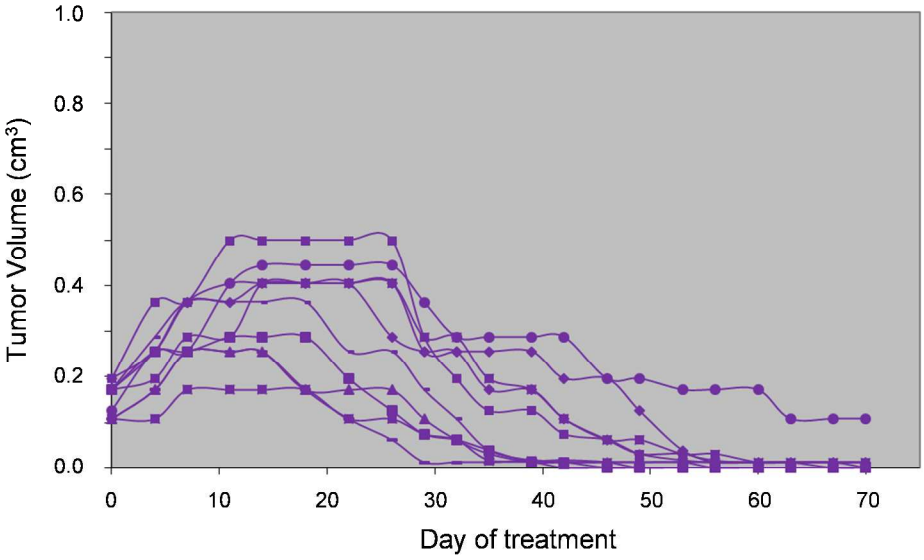

PBPK based modelling predicted that **64** will have a moderate clearance in man (~8 mL/min/kg) and a moderate to high V_{ss} (5.8 L/kg) resulting in a half-life of ~10 hours. Oral bioavailability is predicted to be good (66%) resulting in a predicted efficacious dose of 5 mg QD and a free C_{max} of approximately 0.002 μM. Screening in commercial panels of pharmacologically relevant targets (*e.g.* CEREP panel) suggested that **64** would not exhibit non-ATM mediated pharmacology at this dose (or reasonable multiples thereof). A simulated human pharmacokinetic profile of **64** is shown in figure 8. GI-Sim models predicted that **64** will have a high D_{abs} (>4000 mg) and, therefore, **64** can be considered to have a relatively low risk of being unable to achieve the exposure required to test the biological hypothesis of ATM inhibition in the clinic and is unlikely to require lengthy and costly formulation development. Compound **64** was selected as a clinical candidate and given the identifier AZD0156. The pharmacokinetics of **64** in rat and dog was well behaved and showed broadly dose linear exposure in the range required to enable toxicology studies in these species. The detailed preclinical *in vivo* toxicological evaluation of **64** supported dosing to patients and **64** (AZD0156) is currently under investigation in phase I clinical studies in combination with either olaparib or inrinotecan (ClinicalTrials.gov Identifier: NCT02588105).

Figure 8: PBPK simulation of steady state human exposure following a 6 mg daily oral dose of **64**.

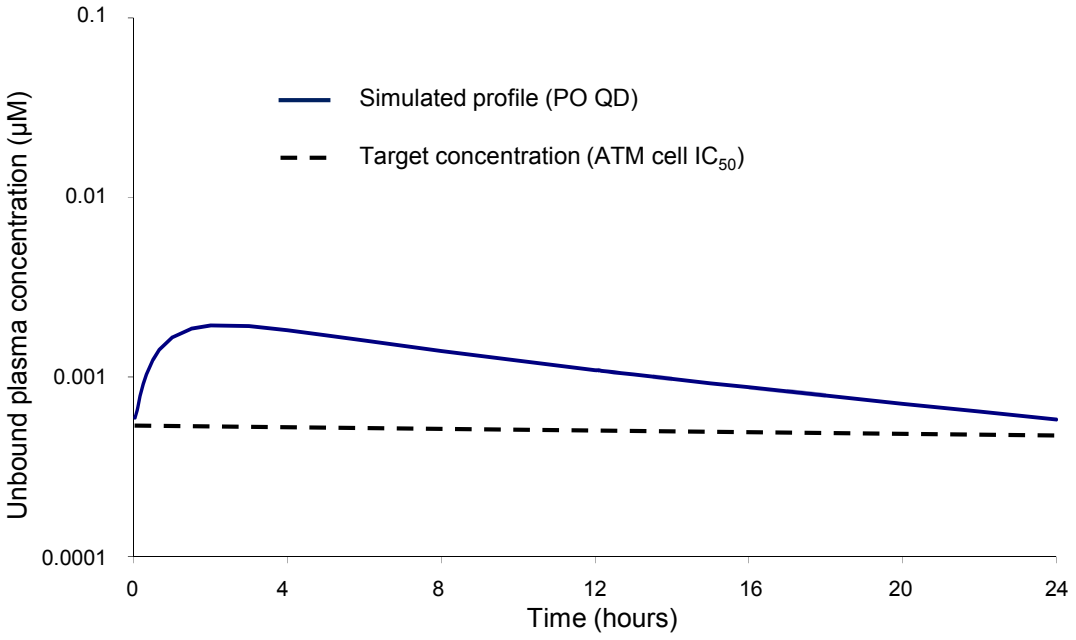

The potential for **64** to generate pharmacologically active metabolites was assessed using *in vitro* metabolite identification studies. These studies determined that a major route of metabolism for **64** in humans was likely to be flavin-containing monooxygenase (FMO) mediated *N*-oxidation of the basic nitrogen moiety leading to the generation of **65**, figure 9. Discrete synthesis and profiling of **65** showed that this metabolite retained activity against ATM, albeit reduced, but remained selective over closely related targets (ATM IC_{50} = 0.005 µM, ATR IC_{50} = 10 µM). Although **65** was less active than the parent molecule, the potential for the metabolite to contribute to efficacy was appreciated; however, metabolic conversion of **64** to generate **65** in hepatocyte incubations was relatively low (≤10% in rat, dog and human hepatocytes) and only low levels were detected in rat and dog *in vivo* studies (<10% of parent by AUC). Based on this data we concluded that the contribution of this metabolite to any observed clinical efficacy was likely to be minor.

Figure 9: Structure of **65**.

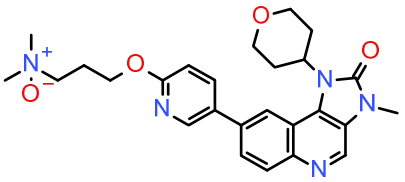

65

Whilst details of the clinical utility of **64** in combination with DNA DSB-inducing therapies will be reported elsewhere, early human pharmacokinetic data is now available. To assess the pharmacokinetic half-life, blood samples were collected from patients' whole blood at predose, 0.25, 0.5, 1, 2, 3, 4, 6, 8, 12, ~24, ~48, and ~72 hours post a single oral dose and at predose, 0.25, 0.5, 1, 2, 3, 4, 6, 8, 12 hours post dose at steady-state following twice daily oral administration. **64** was quantitated in human plasma samples using a fully validated bioanalytical method at Covance Laboratories Limited, Indianapolis, IN, US. The method employs protein precipitation and liquid chromatography followed by tandem mass spectrometric detection (LC-MS/MS).[63] The analytical method has a calibration range of 0.2 to 200 ng/mL and a noncompartmental method was used to derive pharmacokinetic parameters for **64** from plasma concentration-time data using Phoenix® WinNonlin® (version 6.4; Certara, L.P., Princeton, NJ, US). The pharmacokinetic profile of **64** following twice daily oral administration, at steady-state, is shown in figure 10. The terminal half-life at steady-state was between 9 to 12 hours with a median T_{max} between 2.0 to 2.5 hours post dose. The systemic exposure of **64** increased in an approximately dose proportional manner with moderate to high variability, table 10. More detailed studies will be required to better understand the factors governing the clincal exposure of **64**, but it should be noted that the terminal half-life observed is broadly in line with the prediction highlighting the utility of such predictions. It should also be noted that the drive to optimize both the predicted clinical dose and the D_{abs} has resulted in a molecule that has shown broadly dose proportional exposure at doses in excess of the original predicted dose, again highlighting the validity of optimization against these parameters.

Figure 10: Mean (+ standard deviation) plasma concentration (ng/mL) of **64** versus time at steady-state following twice daily oral administration at the dose levels of 15, 30, 60 and 120mg BID in patients with solid tumors.

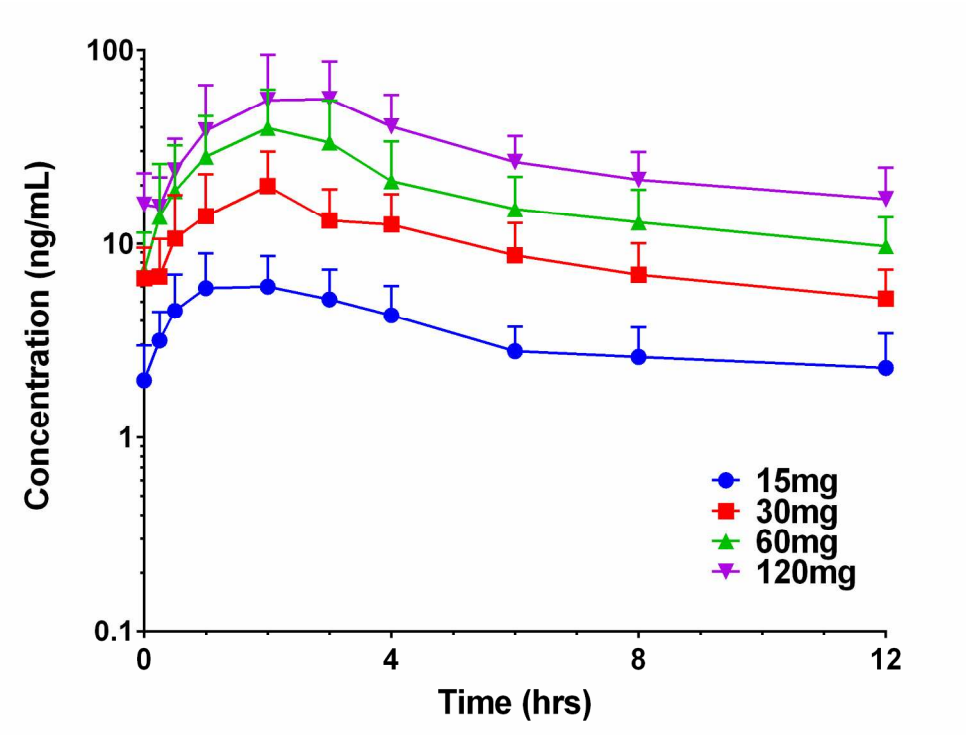

Table 10: Pharmacokinetic parameters of **64** after multiple oral administrations at steady-state in patients with solid tumors.

Dose (mg)	C_{max} (ng/mL)	T_{max} (h)	AUC_{0-12} (ng.h/mL)
15 mg BID (n = 6)	6.67 ± 2.37	2.0	40.35 ± 18.67
30 mg BID (n = 4)	17.46 ± 10.05	2.0	105.10 ± 52.18
60 mg BID (n = 4)	39.63 ± 25.01	2.5	206.30 ± 97.76
120 mg BID (n = 4)	58.83 ± 36.70	2.5	330.20 ± 171.90

Data are mean ± standard deviation with the exception of T_{max} where the data is the median

CONCLUSION

ATM plays a key role in the detection and repair of the cytotoxic DNA DSBs and as such represents an important pharmaceutical target with the potential to increase the efficacy of existing therapies whose mechanism of action involves the induction of DNA DSBs. Previous research within our laboratories had identified the first high quality potent and selective inhibitors of ATM, such as **7**, with properties suitable for oral administration to facilitate *in vivo* target validation. However, concerns around the ability to develop such compounds as clinical candidates resulted in continued optimization with a particular emphasis on reducing the predicted clinical dose and identifying compounds with good developability. The potential to target the optimization of both primary potency and the predicted human pharmacokinetic profile to reduce the predicted clinical dose was appreciated and in particular, given the relatively low hepatic turnover of **7**, we sought to increase V_{ss}. The ability to introduce basic functionality was explored and resulted in the identification of **16** which showed improved ATM potency and increased predicted V_{ss}; however, compromised permeability precluded the further development of this compound. An understanding of the Structure-Property-Relationships for this series revealed a low likelihood of achieving a permeable compound with increased V_{ss} (*i.e.* basic compound) and a scaffold hopping strategy was adopted. Combining knowledge of the predicted binding modes with internal data suggested that the imidazo[5,4-c]quinolin-2-one scaffold may provide a suitable alternative, albeit with reduced selectivity. Optimization of this scaffold resulted in the discovery of permeable compounds with exceptional potency and selectivity and possessing good physicochemical properties. Of these compounds **64** (AZD0156) was considered to have a particularly attractive balance of properties and showed good pharmacokinetics in preclinical studies. **64** is predicted to have a low clinically efficacious dose and is considered unlikely to require detailed formulation work to achieve relevant clinical exposures. In addition, **64** has demonstrated the ability to potentiate the efficacy of DNA DSB inducing agents in disease relevant mouse xenograft models. The early human pharmacokinetic data suggests that the predicted phamacokinetic half-life is broadly in line with the

observed value, thus higlighting the utility of driving optimization based on such parameters. A more detailed understanding of the factors influencing the clincal exposure observed with **64** will no doubt emerge with time but current data supports the continued clincal exploration of **64**, a first in class, potent and selective ATM inhibitor, as a potential cancer therapy.

EXPERIMENTAL SECTION

General Methods. All experiments were carried out under an inert atmosphere and at ambient temperature unless otherwise stated. Microwave reactions were performed using one of the following reactors: Biotage initiator, Personal Chemistry Emrys optimizer, Personal Chemistry Smithcreator, or CEM Explorer. Workup procedures were carried out using traditional phase separating techniques or by using strong cation exchange (SCX) chromatography using Isolute SPE flash SCX-2 column (International Sorbent Technology Limited, Mid Glamorgan, U.K.). When necessary, organic solvents were dried over anhydrous $MgSO_4$ or Na_2SO_4. Flash chromatography purifications were performed on an automated Armen Glider Flash : Spot II Ultimate (Armen Instrument, Saint-Ave, France) or automated Presearch combiflash companions using prepacked Merck normal phase Si60 silica cartridges (granulometry : 15-40 or 40-63µm) obtained from Merck, Darmstad, Germany, siliclyle silica cartridges or graceresolv silica cartridges. Preparative reverse phase HPLC was performed on a Waters instrument (600/2700 or 2525) fitted with a ZMD or ZQ ESCi mass spectrometers and a Waters X-Terra or a Waters X-Bridge or a Waters SunFire reverse-phase column (C-18, 5 microns silica, 19 mm or 50 mm diameter, 100 mm length, flow rate of 40 mL / minute) using decreasingly polar mixtures of water (containing 1% ammonia) and acetonitrile or decreasingly polar mixtures of water (containing 0.1% formic acid) and acetonitrile as eluents. Intermediates were not necessarily purified, but their structures and purity were assessed by TLC, NMR, HPLC and mass spectral techniques and are consistent with the proposed structures. The purity of compounds for biological testing were assessed by NMR, HPLC and mass spectral techniques and are consistent with the proposed structures; purity was ≥95%. Electrospray

mass spectral data were obtained using a Waters ZMD or Waters ZQ LC/mass spectrometer acquiring both positive and negative ion data, and generally, only ions relating to the parent structure are reported; proton NMR chemical shift values were measured on the delta scale using either a Bruker DPX300 spectrometer operating at a field strength of 300 MHz, a Bruker DRX400 operating at 400 MHz, a Bruker DRX500 operating at 500 MHz or a Bruker AV700 operating at 700 MHz. Unless otherwise stated, NMR spectra were obtained at 400 MHz in deuterated dimethylsulfoxide. The following abbreviations have been used: s, singlet; d, doublet; t, triplet; q, quartet; m, multiplet; br, broad; qn, quintet. Compounds were optionally isolated as the methanesulfonate salt by dissolving the isolated base in DCM and treating with 1M methanesufonic acid in DCM (1.1 equiv) and stirring at ambient temperature. The solvent was removed *in vacuo* and if required the residue triturated with diethylether to afford the desired salt. Where the synthesis of an intermediate or reagent is not described then it has either already been described in the literature,[30,61] or is available from commercial sources.

The following abbreviations may be used: Abbreviations: THF = tetrahydrofuran; DIPEA = diisopropylethylamine; DMF = N,N dimethylformamide; DMSO = dimethylsulfoxide; DMA = N,N-dimethylacetamide; DME = 1,2-dimethoxyethane; DCM = dichloromethane; MeOH = methanol;

The preparation of **64** from 8-bromo-3-methyl-1-(oxan-4-yl)imidazo[5,4-c]quinolin-2-one is described below.

8-(6-Fluoropyridin-3-yl)-3-methyl-1-(oxan-4-yl)imidazo[5,4-c]quinolin-2-one (**62**). Monopalladium(IV) disodium tetrachloride (0.02 equiv) was added to 8-bromo-3-methyl-1-(oxan-4-yl)imidazo[5,4-c]quinolin-2-one (1 equiv), (6-fluoropyridin-3-yl)boronic acid (25.7 g, 182.21 mmol), K_2CO_3 (3 equiv) and 3-(di-*tert*-butylphosphino)propane-1-sulfonic acid (0.01 equiv) in 1,4-dioxane and

water at ambient temperature under air. The resulting mixture was stirred at 80°C for 16 hours. The reaction mixture was diluted with water and the precipitate collected by filtration, washed with water and dried under vacuum. The resulting solid was dissolved with DCM and the mixture filtered through celite to remove palladium residues. The solvent was removed under reduced pressure to afford the desired material (96 %). ^{1}H NMR (400MHz, $CDCl_3$) δ 1.85-2.01 (2H, m), 2.86 - 3.02 (2H, m), 3.57 - 3.68 (5H, m), 4.16 - 4.31 (2H, m), 5.11 (1H, t), 6.98 - 7.19 (1H, m), 7.83 (1H, dd), 8.16 (1H, td), 8.30 (1H, dd), 8.50 (1H, s), 8.60 (1H, s), 8.77 (1H, s). m/z (ES+)[M+H]+ = 379

8-[6-[3-(Dimethylamino)propoxy]-3-pyridyl]-3-methyl-1-tetrahydropyran-4-yl-imidazo[4,5-c]quinolin-2-one (**64**). Sodium hydride (60% dispersion in mineral oil) (4 equiv) was added portion-wise to 3-(dimethylamino)propan-1-ol (2 equiv) in DMF (500 mL) at 10°C over a period of 20 minutes under nitrogen. The resulting mixture was stirred at ambient temperature for 1 hour then 8-(6-fluoropyridin-3-yl)-3-methyl-1-(oxan-4-yl)imidazo[5,4-c]quinolin-2-one (1 equiv) was added portion-wise to the reaction mixture at 10°C over a period of 20 minutes under nitrogen. The resulting mixture was stirred at ambient temperature for 16 hours then diluted with water and the precipitate collected by filtration, washed with water and dried under vacuum. The dried solid was triturated with EtOAc, filtered and the solid purified by crystallisation from MeCN to afford the desired product (82%). The material could be converted to a stable crystalline form following suspension in MeCN and stirring at ambient temperature overnight. ^{1}H NMR (400MHz, DMSO-d6) δ 1.81 - 1.99 (4H, m), 2.16 (6H, s), 2.37 (2H, t), 2.73 (2H, qd), 3.51 (3H, s), 3.59 (2H, t), 4.07 (2H, dd), 4.37 (2H, t), 5.14 (1H, ddd), 6.94 - 7.01 (1H, m), 7.95 (1H, dd), 8.14 (1H, d), 8.18 (1H, dd), 8.43 (1H, s), 8.66 (1H, d), 8.89 (1H, s). m/z (ES+)[M+H]+ = 462.6. ^{1}H NMR (700 MHz, $CDCl_3$, 300K) δ 1.94 (dd, J = 4.40, 13.30 Hz, 2H), 1.99 (p, J = 6.97 Hz, 2H), 2.27 (s, 6H), 2.47 (t, J = 7.42 Hz, 2H), 2.96 (qd, J = 4.22, 12.00 Hz, 2H), 3.58 – 3.63 (m, 5H), 4.24 (dd, J = 4.77, 11.88 Hz, 2H), 4.42 (t, J = 6.50 Hz, 2H), 5.08 (t, J = 11.10 Hz, 1H), 6.89 (d, J = 8.55 Hz, 1H), 7.80 (d, J = 8.92 Hz, 1H), 7.92 (dd, J = 2.57, 8.71 Hz, 1H), 8.21 (d, J = 8.84 Hz, 1H),

8.39 (s, 1H), 8.51 (d, J = 2.56 Hz, 1H), 8.70 (s, 1H); ^{13}C NMR (176 MHz, $CDCl_3$, 300K) δ 27.59, 30.41, 45.68, 53.48, 56.62, 64.85, 67.87, 111.56, 116.00, 118.48, 123.65, 125.87, 129.07, 129.34, 132.28, 132.50, 136.26, 137.45, 144.90, 145.45, 153.74, 164.04; HRMS (ESI^+): Anal calcd for ($M+H^+$): C26H31N5O3 462.24997, Found: 462.25024. The absolute purity of the sample was determined to be 99.6% w/w ± 2% by by absolute Internal Calibrant qNMR (spectra available in supporting information).

ASSOCIATED CONTENT

Supporting Information

Experimental procedures for the key biological assays, the synthesis and analytical data of final compounds and key intermediates, experimental procedure and data for the NMR structural and conformational elucidation of **64**, the purity assessment of **64**, the kinome selectivity data for **64**, the coordinates for the homology model and a file of the molecular formular strings of the molecules described can all be found in the supporting information.

AUTHOR INFORMATION

Corresponding Author

* Phone: +44 (0)1223 223440. E-mail: kurt.pike@astrazeneca.com

Notes

The authors declare no competing financial interest.

ACKNOWLEDGMENT

The authors would like to acknowledge the contribution of Aurelien Peru, Franck Lach, Janet Hawkins, Rosemary Croft, Anil Patel, Jonathan Burgess and Stuart Wells for their contribution to chemical synthesis; to Anna Cronin and Lyn Rosenbrier-Ribeiro for their assistance analyzing secondary pharmacology risks; Ian Barrett and Caroline Truman for their input into assay design and data generation; and to Philip Jewsbury for helpful discussions regarding the manuscript.

ANCILLARY INFORMATION

The following abbreviations may be used: Abbreviations: ATM = Ataxia Telangiectasia Mutated; DSB = double-strand breaks; HRR = homologous recombination repair; NHEJ = non-homologous end-joining; IR = ionizing radiation; PBPK = Physiologically-based pharmacokinetic; D_{abs} = maximum absorbable dose; eD2M = early dose to man prediction; GSF = Simulated Gastric Fluid; FaSSIF = Fasted State Simulated Intestinal Fluid; THF = tetrahydrofuran; DIPEA = diisopropylethylamine; DMF = N,N dimethylformamide; DMSO = dimethylsulfoxide; DMA = N,N-dimethylacetamide; DME = 1,2-dimethoxyethane; DCM = dichloromethane; MeOH = methanol;

REFERENCES

(1) Jackson, S. P.; Bartek, J. The DNA damage response in human biology and disease. *Nature* **2009**, *461*, 1071-1078.

(2) Ciccia, A.; Elledge, S. J. The DNA damage response: making it safe to play with knives. *Mol. Cell* **2010**, *40*, 179-204.

(3) Hoeijmakers, J. H. Genome maintenance mechanisms for preventing cancer *Nature* **2001**, *411*, 366-374.

(4) Shibata, A.; Jeggo, P. A. DNA Double-strand break repair in a cellular context. *Clin. Oncol*. **2014**, *26*, 243-249.

(5) Radhakrishnan, S. K.; Jette, N.; Lees-Miller, S. P. Non-homologous end joining: emerging themes and unanswered questions. *DNA repair (Amst.)* **2014**, *17*, 2-8.

(6) O'Connor, M. J. Targeting the DNA Damage response. *Mol. Cell Rev*. **2016**, *60*, 547-560.

(7) Shiloh, Y. Ataxia-telangiectasia and the Nijmegen breakage syndrome: related disorders but genes apart. *Annu. Rev. Genet*. **1997**, *31*, 635-662.

(8) Fruman, D. A.; Meyers, R. E.; Cantley, L. C. Phosphoinositide Kinases. *Annu. Rev. Biochem*. **1998**, 481-507.

(9) Shiloh, Y. ATM and related protein kinases: safeguarding genome integrity. *Nat. Rev. Cancer* **2003**, *3*, 155-168.

(10) Ditch, S.; Paull, T. T. The ATM protein kinase and cellular redox signaling: beyond the DNA damage response. *Trends in Biochemical Sciences* **2012**, *37(1)*, 15-22.

(11) Andrs, M.; Korabecny, J.; Nepovimova, E.; Jun, D.; Hodny, Z.; Moravcova, S.; Hanzlikova, H.; Kuca, K. The development of ataxia telangiectasia mutated kinase inhibitors. *Mini-reviews in Medicinal Chemistry* **2014**, *14*, 805-811.

(12) Lee, J. H.; Paull, T. T. ATM Activation by DNA double-strand breaks through the Mre11-Rad50-Nbs1 complex. *Science* **2005**, *308 (5721)*, 551-554.

(13) Bakkenist, C. J; Kastan, M. B. DNA Damage activates ATM through intermolecular autophosphorylation and dimer dissociation. *Nature* **2003**, *421*, 499-506.

(14) Burma, S.; Chen, B. P.; Murphy, M.; Kurimasa, A.; Chen, D. J. ATM Phosphorylates histone H2AX in response to DNA double-strand breaks. *Journal of Biological Chemistry* **2001**, *276(45)*, 42462-42467.

(15) Scully, R.; Xie, A. Double strand break repair functions of histone H2AX. *Mutation research* **2013**, *750(1-2)*, 5-14.

(16) Banin, S.; Moyal, l.; Shieh, S. -Y.; Taya, Y.; Anderson, C.W.; Chessa, L.; Smorodinsky, N. I.; Prives, C.; Reiss, Y.; Shiloh, Y. Ziv, Y. Enhanced phosporylation of p53 by ATM in response to DNA damage. *Science* **1998**, *281(5383)*, 1674-1677.

(17) Matsuoka, S.; Huang, M.; Elledge, S. J. Linkage of ATM to cell cycle regulation by the Chk2 protein kinase. *Science* **1998**, *282(5395)*, 1893-1896.

(18) Marine, J. -C.; Lozano, G. Mdm2-Mediated ubiquitylation: p53 and beyond. *Cell Death and Differentiation* **2010**, *17(1)*, 93-102.

(19) Kastan, M. Ataxia-telangiectasia-broad implications for a rare disorder. *N. Engl. J. Med*. **1995**, *333*, 622-663

(20) Moding, E. J.; Kastan, M. B.; Kirsch, D. G. Strategies for optimizing the response of cancer and normal tissues to radiation. *Nat. Rev. Drug Discovery* **2013**, *12*, 526-542.

(21) Cremona, C. A.; Behrens, A. ATM Signaling and cancer. *Oncogene* **2014**, *33(26)*, 3351-3360.

(22) Sarkaria, J. N.; Eshleman, J. S. ATM as a target for novel radiosensitizers. *Semin. Radiat. Oncol*. **2001**, *11*, 316-327.

(23) Zhu, Y.; Hu, J.; Hu, Y.; Liu, W. Targeting DNA repair pathways: a novel approach to reduce cancer therapeutic resistance. *Cancer treat. Rev.* **2009**, *35*, 590-596.

(24) O'Connor, M. J.; Martin, N. M.; Smith, G. C. Targeted cancer therapies based on the inhibition of DNA strand break repair. *Oncogene* **2007**, *26*, 7816-7824.

(25) Hollick, J. J.; Rigoreau, L. J. M.; Cano-Soumillac, C.; Cockcroft, X.; Curtin, N. J.; Frigerio, M.; Golding, B. T.; Guiard, S.; Hardcastle, I. R.; Hickson, I.; Hummersone, M. G.; Menear, K. A.; Martin, N. M. B.; Matthews, I.; Newell, D. R.; Ord, R.; Richardson, C. J.; Smith, G. C. M.; Griffin, R. J. Pyranone, thiopyranone, and pyridone inhibitors of phosphatidylinositol 3-kinase related kinases. Structure-activity relationships for DNA-dependent protein kinase inhibition, and identification of the

first potent and selective inhibitor of the ataxia telangiectasia mutated kinase. *J. Med. Chem*. **2007**, *50*, 1958-1972.

(26) Smith, G. C. M.; Martin, N. M. B.; Jackson, S. P.; O'Connor, M. J.; Lau, A. Y. K. Cockcroft, X. -L. F.; Matthews, I. T. W.; Menear, K. A.; Rigoreau, L. J. M.; Hummersone, M. G.; Girffin, R. J. Pyranones Useful as ATM Protein Kinase Inhibitors, WO 2003070726, Aug 28, 2003.

(27) Hickson, I.; Zhao, Y.; Richardson, C. J.; Green, S. J.; Martin, N. M. B.; Orr, A. I.; Reaper, P. M., Jackson, S. P.; Curtin, N. J.; Smith, G. C. M. Identification and characterization of a novel and specific inhibitor of the ataxia-telangiectasia mutated kinase ATM. *Cancer Research* **2004**, *64*, 9152-9159.

(28) Batey, M. A.; Zhao, Y.; Kyle, S.; Richardson, C.; Slade, A.; Martin, N. M.; Lau, A.; Newell, D. R.; Curtin, N.J. Preclinical evaluation of a novel ATM inhibitor, KU-59403, in vitro and in vivo in p53 functional and dysfunctional models of human cancer. *Mol. Cancer Ther*. **2013**, *12(6)*, 959-967.

(29) Min, J.; Guo, K.; Suryadevara, P. K.; Zhu, F.; Holbrook, G.; Chen, Y.; Feau, C.; Young, B. M.; Lemoff, A.; Connelly, M. C.; Kastan, M. B.; Guy, R. K. Optimization of a novel series of ataxia-telangiectasia mutated kinase inhibitors as potential radiosensitizing agents. *J. Med. Chem*. **2016**, *59*, 559-577.

(30) Degorce, S. L.; Barlaam, B.; Cadogan, E.; Dishington, A.; Ducray, R.; Glossop, S. C.; Hassall, L. A.; Lach, F.; Lau, A.; McGuire, T. M.; Nowak, T.; Ouvry, G.; Pike, K. G.; Thomason, A. G. Discovery of novel 3-quinoline carboxamides as potent, selective and orally bioavailable inhibitors of ataxia telangiectasia mutated (ATM) kinase. *J. Med. Chem*. **2016**, *59*, 6281-6292.

(31) Karlin, J.; Allen, J.; Odedra, R.; Hughes, G.; Farrington, P.; Ducray, R.; Ouvry, G.; Degorce, S.; Wilson, J.; Smith, A.; Patel, B.; Thomason, A.; Vincent, J.; Colclough, N.; Ahmad, S.F.; Beckta, J.M.; Tokarz, M.; Mukhopadhyay, N. D.; Barlaam, B.; Pike, K. G.; Cadogan, E.; Pass, M.; Valerie, K.; Durant, S., Blood-Brain Barrier penetrating ATM Inhibitor Radio-Sensitizes Intracranial Gliomas in

Mice. *Abstracts of papers*, Annual Meeting of the American Association of Cancer Research, New Orleans, LA, 2016.

(32) Pike, K. G., Barlaam, B.; Colclough, N.; McGuire, T. M.; Cadogan, E.; Pass, M.; Hassall, L. A.; Hawkins, J.; Holmes, J.; Dishington, A.; Robb, G.; Ducray, R.; Ouvry, G.; Degorce, S. L.; Lau, A.; MacFaul, P.; Hughes, G. Identifying High Quality, Potent and Selective Inhibitors of ATM Kinase: Discovery of AZD0156. RSC-SCI Kinase 2016, Nottingham, UK, 2016.

(33) Redfern, W. S.; Carlsson, L.; Davis, A. S.; Lynch, W. G.; MacKenzie, I.; Palethorpe, S.; Siegl, P. K. S.; Strang, I.; Sullivan, A. T.; Wallis, R.; Camm, A. J.; Hammond, T. G. Relationships between preclinical cardiac electrophysiology, clinical QT interval prolongation and torsade de pointes for a broad range of drugs: evidence for a provisional safety margin in drug development. *Cardiovasc. Res*. **2003**, *58*, 32-45.

(34) Leahy, D. E.; Arundel, P. A.; Blakey, G. E.; Rowland, M. Physiologic based pharmacokinetic modeling and QSAR. *Bioactive Compound Design* **1996**, 147-151.

(35) Nestorov, I. A.; Aarons, L. J.; Arundel, P. A.; Rowland, M. Lumping of whole-body physiologically based pharmacokinetic models. *Journal of Pharmacokinetics and Biopharmaceutics* **1998**, *26(1)*, 21-46.

(36) McGinnity, D. F.; Collington, J.; Austin, R. P.; Riley, R. J. Evaluation of human pharmacokinetics, therapeutic dose and exposure predictions using marketed oral drugs. *Curr. Drug Metab*. **2007**, *8*, 463−479.

(37) Nakayama, S.; Astumi, R.; Takakusa, H.; Kobayashi, Y.; Kurihara, A.; Nagai, Y.; Nakai, D.; Okazaki, O. A zone classification system for risk assessment of idiosyncratic drug toxicity using daily dose and covalent binding. *Drug Metabolism and Disposition* **2009**, *37(9)*, 1970 – 1977.

(38) Chen, M.; Borlak, J.; Tong, W. High lipophilicity and high daily dose of oral medications are associated with significant risk for drug-induced liver injury. *Hepatology* **2013**, *58*, 388 – 396.

(39) K. C. Johnson, K. C.; Swindell, A. C. Guidance in the setting of drug particle size specification to minimize variability in absorption. *Pharm. Res*. **1996**, *3*, 1795–1798.

(40) Hilgers A. R.; Smith D. P.; Biermacher J. J.; Day J. S.; Jensen J. L.; Sims S. M.; Adams W. J.; Friis J. M.; Palandra J.; Hosley J. D.; Shobe, E. M.; Burton, P. S. Predicting oral absorption of drugs: a case study with a novel class of antimicrobial agents. *Pharmaceutical Research* **2003**, *20(8)*, 1149-1155.

(41) Ding, X.; Rose, J. P.; Van Gelder, J. Developability assessment of clinical drug products with maximum absorbable doses. *International Journal of Pharmaceutics* **2012**, *427(2)*, 260-269.

(42) Sjogren, E.; Westergren, J.; Grant, I.; Hanisch, G.; Lindfors, L.; Lennernas, H.; Abrahamsson, B.; Tannergren, C. In silico predictions of gastrointestinal drug absorption in pharmaceutical product development: application of the mechanistic absorption model GI-Sim. *European Journal of Pharmaceutical Sciences* **2013**, *49*, 679-698.

(43) Hofmann, A. W. On the action of bromine in alkaline solution on amides. *Ber. Dtsch. Chem. Ges*. **1881**, *55*, 2725–2736. (title translated from "Ueber die Einwirkung des Broms in alkalischer Lösung auf Amide")

(44) Ishiyama, T.; Murata, M.; Miyaura N. Palladium(0)-catalyzed cross-coupling reaction of alkoxydiboron with haloarenes: a direct procedure for arylboronic esters. *J. Org. Chem*. **1995**, *60*, 7508-7510.

(45) Page, K. M. Validation of early human dose prediction: a key metric for compound crogression in drug discovery. *Molecular Pharmaceutics* **2016**, *13(2)*, 609-620.

(46) Smith, D. A.; Beaumont, K.; Maurer, T. S.; Di, L. Volume of distribution in drug design. *J. Med. Chem*. **2015**, *58*, 5691-5698.

(47) Furet, P.; Caravatti, G.; Guagnano, V.; Lang, M.; Meyer, T.; Schoepfer, J. Entry into a new class of protein kinase inhibitors by pseudo ring design. *Bioorganic and Medicinal Chemistry Letters* **2008**, *18*, 897 – 900.

(48) Maria, S. M.; Stauffer, F.; Brueggen, J.; Furet, P.; Schnell, C.; Fritsch, C.; Brachmann, S.; Chene, P.; De Pover, A.; Schoemaker, K.; Fabbro, D.; Gabriel, D.; Simonen, M.; Murphy, L.; Finan, P.; Sellers, W.; García-Echeverría, C. Identification and characterization of NVP-BEZ235, a new orally available dual phosphatidylinositol 3-kinase/mammailian target of rapamycin inhibitor with potent in vivo antitumor activity. *Mol. Can. Ther*. **2008**, *7(7)*, 1851-1863.

(49) Gil del Alcazar, C. R.; Hardebeck, M. C.; Mukherjee, B.; Tomimatsu, N.; Gao, X.; Yan, J.; Xie, X.-J.; Bachoo, R.; Li, L.; Habib, A. A.; Habib, S. B. Inhibition of DNA double-strand break repair by the dual PI3K/mTOR inhibitor NVP-BEZ235 as a strategy for radiosensitization of glioblastoma. *Clin. Cancer Res.* **2014**, *20(5)*, 1235-1248.

(50) Mukherjee, B.; Tomimatsu, N.; Amancherla, K.; Camacho, C.V.; Pichamoorthy, N.; Burma, S. The dual PI3K/mTOR inhibitor NVP-BEZ235 is a potent inhibitor of ATM- and DNA-PKcs-mediated DNA damage responses. *Neoplasia* **2012**, *14*, 34-43.

(51) Tarcsay, A.; Nyiri, K.; Keseru, G. M. Impact of lipophilic efficiency on compound quality. *J. Med. Chem.* **2012**, *55*, 1252–1260.

(52) Murray, C. W.; Erlanson, D. A.; Hopkins, A. L.; Keseru, G. M.; Leeson, P. D.; Rees, D. C.; Reynolds, C. H.; Richmond, N. J. Validity of ligand efficiency metrics. *Med. Chem. Lett*. **2014**, *5*, 616-618.

(53) Free, S. M., Jr.; Wilson, J. W. A mathematical contribution to structure−activity studies. *J. Med. Chem*. **1964**, *7*, 395−399.

(54) Waring, M. J.; Johnstone, C.; McKerrecher, D.; Pike, K. G.; Robb, G. Matrix-based multiparameter optimisation of glucokinase activators: the discovery of AZD1092. *MedChemComm* **2011**, *2*, 775-779.

(55) Freeman-Cook, K. D.; Amor, P.; Bader, S.; Buzon, L. M.; Coffey, S. B.; Corbett, J. W.; Dirico, K. J.; Dorn, S. D.; Elliott, R. L.; Esler, W.; Guzman-Perez, A.; Henegar, K. E.; Houser, J. A.; Jones, C. S.;Limberakis, C.; Loomis, K.; McPherson, K.; Murdande, S.; Nelson, K. L.; Phillion, D.; Pierce, B. S.;

Song, W.; Sugarman, E.; Tapley, S.; Tu, M.; Zhao, Z. Maximising lipophilic efficiency: the use of Free−Wilson analysis in the design of inhibitors of acetyl-CoA carboxylase. *J. Med. Chem*. **2012**, *55*, 935−942.

(56) Goldberg, F. W.; Leach, A. G.; Scott, J. S.; Snelson, W. L.; Groombridge, S. D.; Donald, C. S.; Bennett, S. N. L.; Bodin, C.; Morentin Gutierrez, P.; Gyte, A. C. Free−Wilson and structural approaches to co-optimizing human and rodent isoform potency for 11β-hydroxysteriod dehydrogenase type 1 (11β-HSD1) inhibitors. *J. Med. Chem*. **2012**, *55*, 10652−10661.

(57) Pike, K. G.; Morris, J.; Ruston, L.; Pass, S. L.; Greenwood, R.; Williams, E. J.; Demeritt, J.; Culshaw, J. D.; Gill, K.; Pass, M.; Finlay, M. R. V.; Good, C. J.; Roberts, C. A.; Currie, G. S.; Blades, K.; Eden, J. M.; Pearson, S. E. Discovery of AZD3147: A potent, selective dual inhibitor of mTORC1 and mTORC2. *J. Med. Chem*. **2015**, *58*, 2326-2349.

(58) Blundell, C. D.; Packer, M. J.; Almond, A. Quantification of free ligand conformational preferences by NMR and their relationship to the bioactive conformation. *Bioorg. Med. Chem*. **2013**, *21*, 4976 – 4987.

(59) Cadogan, E. D. Discovery and Preclinical Pharmacology of AZD0156: a First in Class Potent and Selective Inhibitor of Ataxia Telangiectasia Mutated (ATM) Kinase. *Abstracts of papers*, Annual Meeting of the American Association of Cancer Research, New Orleans, LA, 2016.

(60) Riches, L. C.; Hughes, G.; Jones, G. N.; Garcia-Trinidad, A.; Thomason, A. G.; Gavine, P.; Cui, A.; O'Connor, M.; Ling, S.; Stott, J.; Clark, R.; Peel, S.; Gill, P.; Goodwin, L.; Pike, K. G.; Pass, M.; Barlaam, B.; Smith, G.; Cadogan, E. B. unpublished results.

(61) Barlaam, B. C.; Pike, K. G. Imidazo[4,5-c]quinolin-2-one Compounds and Their Use in Treating Cancer. WO 2015170081, Nov 12, 2015.

(62) Ellison, G.; Huang, S.; Carr, H.; Wallace, A.; Ahdesmaki, M.; Bhaskar, S.; Mills, J. A reliable method for the delection of BRCA1 and BRCA2 mutations in fixed tumour tissue utilizing multiplex PCR-based targeted next generation sequencing. *BMC Clinical Pathology* **2015**, *15*, 1-14.

(63) Kowalski, K.; Hansen, P.; Dayton, B.; Oladipupo, O.; Thomas, E.; Li, Y.; Chen, Y. Overcoming Matrix-Based Interferences Using Multi-Extraction Techniques for LC-MS Analysis of AZD0156 and its Metabolite in Human Plasma. 65th American Society for Mass Spectrometry Annual Conference (ASMS 2017); Indianapolis, IN, 2017.

TABLE OF CONTENTS GRAPHIC

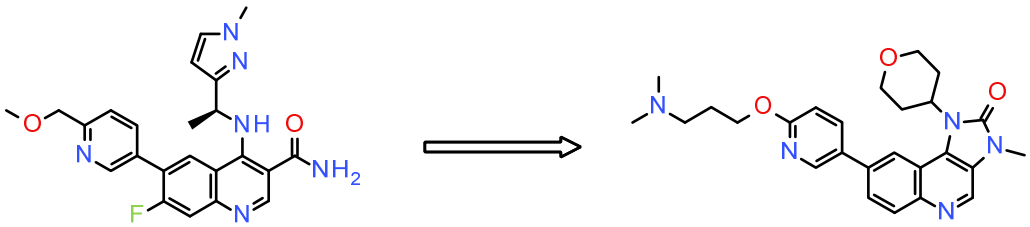

7
ATM IC_{50} = 0.033 μM
Pred Dose = 700 mg QD

64 (AZD0156)
ATM IC_{50} = 0.00058 μM
Pred Dose = 5 mg QD